**Full Paper**

# Ordered Porous Electrodes by Design: Towards Enhancing the Effective Utilization of Platinum in Electrocatalysis

*Brandy K. Pilapil[1], Julia van Drunen[2], Yoseif Makonnen[2], Diane Beauchemin[2], Gregory Jerkiewicz[2], Byron D. Gates[1]**

[1] B. K. Pilapil, B. D. Gates
Department of Chemistry and 4D LABS Simon Fraser University, 8888 University Dr. Burnaby BC, V5A 1S6, Canada

* E-mail: bgates@sfu.ca

[2] J. van Drunen, Y. Makonnen, D. Beauchemin, G. Jerkiewicz
Department of Chemistry Queen's University, 90 Bader Lane Kingston ON, K7L 3N6, Canada

Keywords: self-assembly; structure-property relationships; catalysis; fuel cells; porous electrodes

Final version published as: Ordered Porous Electrodes by Design: Toward Enhancing the Effective Utilization of Platinum in Electrocatalysis, Pilapil, B.K.; Drunen, J. van; Makonnen, Y.; Beauchemin, D.; Jerkiewicz, G.; Gates, B.D., *Advanced Functional Materials*, 2017, 27 (36), 1703171. https://doi.org/10.1002/adfm.201703171

Platinum nanoparticle functionalized ordered porous support electrodes are prepared and characterized as a potential new class of oxygen reduction reaction (ORR) electrocatalysts. This study aims to develop electrode materials that enhance the effective utilization of Pt in electrocatalytic reactions through improved mass transport properties, high Pt mass specific surface area, and increased Pt electrochemical stability. The electrodes are prepared using modular sacrificial templates, producing a uniform distribution of Pt nanoparticles inside ordered porous Au electrodes. This method could be further fine-tuned to optimize the architecture for a range of characteristics, such as varying nanoparticle properties, pore size or support material. The Pt coated Au ordered porous electrodes exhibit several improved characteristics, such as enhanced Pt effective utilization for ORR electrocatalysis. This includes a nearly two fold increase in Pt mass specific surface area over other ultrathin designs, superior mass transport properties in comparison to traditional catalyst layers of C black supported Pt nanoparticles mixed with ionomer, good methanol tolerance and exceptional stability towards Pt chemical and/or electrochemical dissolution through interfacial interactions with Au. The methods to prepare Pt coated ordered porous electrodes could be extended to other architectures for enhanced catalyst utilization and improved performance of Pt in electrochemical processes.

## 1. Introduction

Platinum is a great electrocatalyst for a range of reactions due to its relative chemical stability and high surface energy.[1, 2] However, the high cost and limited supplies of Pt limit its broad use in commercial applications. Designing electrocatalysts that efficiently utilize Pt can reduce material costs and enable commercial success for a wide variety of electrochemical technologies, such as low temperature or polymer electrolyte membrane (PEM) fuel cells (FCs). The effective utilization of Pt encompasses a range of different factors, including: (i) Pt surface area to mass ratio (mass specific surface area); (ii) stability under electrochemical conditions (corrosion resistance); (iii) interfacial interactions with the catalyst support; and (iv) mass transport of reactants and products between the electrode surfaces and the electrolyte bulk. The most commonly applied commercial fuel catalyst layer designs consist of Pt nanoparticles (NPs) dispersed over the surfaces of interconnected C black particles in a matrix of ionomer. These catalyst layers can achieve a very high Pt mass specific surface area (>100 $m^2/g_{Pt}$), but commonly suffer from poor stability and fluctuating mass transport properties, resulting in Pt losses through chemical and/or electrochemical dissolution and under-utilization of the incorporated Pt catalyst. The cathodic catalyst layer (CCL) is of particular concern in PEMFCs, owing to the poor kinetics of the oxygen reduction reaction (ORR) resulting in a large overpotential ($\eta$) and a correspondingly high mass of Pt required at the CCL in order to achieve appreciable currents.[1, 3] Limited transport of reactants and products in the CCL results in a significant portion of the Pt catalyst remaining unused in electrochemical reactions.[4, 5, 6] In addition to these limitations Pt losses can occur due to chemical and/or electrochemical dissolution of Pt and its oxide, and mobility of Pt NPs, resulting in the loss of Pt particles to the effluent or membrane, as well as NP aggregation or NP agglomeration.[7, 8] Direct methanol fuel cells (DMFCs) have additional constraints for the CCL relating to the use of methanol (MeOH) as a fuel, as opposed to $H_2$ gas used in typical PEMFCs. Among these issues, methanol

crossover from the anode to the cathode lowers the overall power density achieved in DMFCs and limits its commercial viability.[9, 10] Improvements to the CCL design are, therefore, necessary to efficiently and effectively utilize Pt and to ultimately minimize the Pt mass loading requirements.

Ultrathin (<1 μm) CCL designs, such as those produced by 3M Inc. and their collaborators,[11, 12] can enhance Pt utilization in comparison to traditional carbon black supported Pt NP designs. These enhancements are believed to result from the improved mass transport properties of the layer due to the significant reduction in catalyst layer thickness and increased catalyst stability arising from the presence of Pt in a highly agglomerated form (as opposed to a dispersion of NPs).[1, 11, 12] Despite these improvements, the required platinum group metals (PGMs) loading continues to exceed the current U.S. Department of Energy 2017 targets of 0.125 mg/cm$^2$ for electrocatalysts (cathode and anode) in stacks rated to produce power densities of 8.0 kW/$g_{Pt}$.[1, 13] The relatively high loading of Pt in these ultrathin CCLs is in part due to the relatively low mass specific surface areas achieved in this design (generally less than 20 m$^2$/$g_{Pt}$), as well as issues related to water management.[1, 11] Overall, catalyst designs with a relatively large void space (e.g., ~60%),[5] minimal electrode thickness (e.g., <5 μm),[4, 12] good porous interconnectivity, high Pt stability under electrocatalytic conditions and a high Pt mass specific surface area are sought to enhance the effective utilization of Pt within new electrocatalyst designs.[1-3, 8, 14, 15, 16] In addition, improvements to the MeOH tolerance of Pt-based electrode designs could enhance their performance as CCLs in DMFCs.

The new class of ultrathin electrodes developed in this work aim to maximize the effective utilization of Pt in electrochemical reactions. These ultrathin ordered porous supports are prepared with a uniform coverage of Pt nanoparticles. Improvement to the mass transport properties and Pt utilization in ultrathin CCLs is pursued through the use of an ordered porous scaffold with a large yet mesoscopic void space. An ordered porous scaffold of electrodeposited

Pt has previously been shown to exhibit enhanced performance at high current densities, which was attributed to its intrinsic morphological advantages.[17] Further enhancements to the Pt mass specific surface area and Pt stability are sought herein through the use of small Pt NPs uniformly distributed over a conductive support material, which exhibits favorable interfacial interactions with the Pt NPs, as to minimize Pt losses while increasing its effective utilization.[1, 13, 18] A new class of electrodes were prepared through the use of a modular sacrificial template, as depicted in **Figure 1**, providing control over catalyst layer thickness and porosity.[19] It should be noted that the gold support material demonstrated here serves as a model and could be readily exchanged for other materials (e.g., to minimize cost and optimize interfacial interactions). However, gold was chosen in this demonstration for its relatively high corrosion resistance, high electrical conductivity and ability to stabilize small Pt clusters through electronic interactions.[18] The size and connectivity of the pores within the ordered porous electrode may be further tuned through the use of spherical templates of varying dimensions,[20] while the NP properties (e.g., size, surface coverage, NP-to-NP spacing) may be optimized through tuning of the pre-formed spherical template.[21] Overall, the work shown here aims to demonstrate the modular preparation of Pt-coated ordered porous electrodes and their potential as electrocatalysts with improved effective utilization of Pt through high electrochemical stability, good methanol tolerance, large Pt mass specific surface area and enhanced mass transport.

## 2. Results and Discussion

The Pt-coated ordered porous electrodes were prepared through a modular sacrificial template method.[19] Platinum NPs with a diameter of 2.6 ± 0.4 nm were uniformly assembled onto the surfaces of ~420-nm diameter amine-functionalized polystyrene (PS) spheres. Details about this assembly have been described in our previous work.[21] Nanoparticle loadings of 1 NP per 59 ± 4 $nm^2$ were achieved on the surfaces of the PS spheres along with an interparticle spacing of 9 ± 2 nm. These NP-coated PS spheres were assembled into an ordered array that served as

a template to the ordered porous electrode materials. Gold was subsequently electrodeposited through the ordered template of Pt NP-coated PS spheres. The PS sphere template was dissolved in organic solvents to reveal the Pt NPs covering the surfaces of an ordered porous network. To our knowledge, this is the first demonstration of the use of NP-coated spherical templates in the preparation of NP-functionalized ordered porous materials. The Pt NPs transfer from the surfaces of the PS spheres to the surfaces of the gold electrodes as a result of partial encapsulation of the Pt NPs by the electrodeposited Au. The Pt NPs extend from the surfaces of the PS spheres upon which they were assembled, rather than being embedded within the PS matrix (Figure S1 in Supporting Information). The Au is in intimate contact with these Pt NPs as a result of the Au electrodeposition through the ordered template of PS spheres. The polyvinylpyrrolidone (PVP) coating on the Pt NPs may facilitate a partial encapsulation of the NPs by Au electrodeposition due to favorable interactions between the Au and the PVP.[22] Previous reports have demonstrated the preparation of NP-coated hollow insulating ceramic spheres by sol-gel methods.[23] In addition, NP-functionalized ordered porous (OP) materials have been previously prepared by forming the NPs *in situ* through the reduction of metal salts onto a pre-formed OP framework (via calcining, photodeposition, or electroless methods).[24] The method demonstrated here, whereby NPs are transferred from a PS template into the OP support, provides much greater control over NP properties, including the NP size, composition, and loading of NPs, as well as the NP-to-NP spacing. These properties can be tuned at the stage when preparing the NP coating on the sacrificial template prior to use as a pore forming template. The approach to preparing electrodes reported in this contribution generates electrocatalytic materials possessing a unique set of structural and catalytic properties that will be discussed below. Scanning electron microscopy (SEM) images of the Pt-coated ordered porous Au electrodes show the 3D ordered porous Au network, with uniform pore sizes and a high-degree of interconnectivity, and the successful transfer of Pt NPs from the spherical PS templates to this framework (**Figure 2**). The uniform porosity of these electrodes is essential to

achieve even transport properties, while uniform interconnectivity facilitates electrical conductivity and creates favorable conditions for utilization of all Pt NPs. Analysis by transmission electron microscopy (TEM) of a fragment of the Pt-coated ordered porous Au electrodes was necessary to image the Pt NPs on the Au surfaces (due to the limits in spatial resolution of the SEM tool used in these studies). These TEM images indicate the presence of large Au grains with small, dark "spots" visible in regions near to the center of the image, where the Au is thinnest for this section of the support. Similarly, scanning TEM (STEM) images from the same section of this Pt-coated ordered porous Au electrode contain small, brighter spots near the same thin region at the center of the image. The size of these spots is in agreement with the original dimensions of the Pt NPs (2.4 ± 0.3 nm in diameter, Figure S2 in Supporting Information). In addition, the contrast observed in both TEM and STEM analyses corresponds to that expected for Pt NPs. A shorter inelastic mean free path is anticipated for high energy electrons in the Pt NPs (attributed to a higher electron density) than for the Au support, indicating that these "spots" are indeed Pt NPs.[25] Additional TEM data is shown in the supplementary material, which reveals a statistically identical surface coverage of NPs on the spherical PS template and after transfer to the Au support. The transfer of NPs from the PS template to the porous Au support was further demonstrated by X-ray photoelectron spectroscopy (XPS) and cyclic voltammetry (CV) analyses, as described in the supplementary material. A Pt surface coverage of at least 15 ± 4% was consistently demonstrated by a series of analytical techniques (i.e. separate results from TEM, XPS and CV measurements). In summary, these analyses suggest a quantitative transfer of Pt NPs from the spherical templates, with negligible loss of Pt NPs and minimal changes to the characteristics of the NPs and their distribution on the surfaces.

Achieving a large Pt mass specific surface area ($A_{ecsa,Pt}/g_{Pt}$) is a challenge for ultrathin catalyst layer designs.[1, 6, 11, 17, 19] Traditional catalyst layers prepared from a mixture of C black

supported Pt NPs with ionomer can readily achieve values in excess of 40 $m^2$ per $g_{Pt}$, while ultrathin designs typically achieve values only between 5 and 20 $m^2$ per $g_{Pt}$.[1, 26] Developing electrocatalyst architectures with a high Pt mass specific surface area, while maintaining an ultrathin design and the associated improvements in mass transport properties, poses a major challenge that, if successfully addressed, could result in new types of electrocatalytic materials with significantly improved performance. Mass analysis by inductively coupled plasma mass spectrometry (ICP-MS) of the Pt-coated ordered porous Au electrodes, conducted for the first time for this type of material, indicates that each electrode contained a Pt mass of 0.0033 ± 0.0005 mg $cm^{-2}$ as determined on the basis of the geometrical area of the electrode ($A_{geom}$) and a Au mass of 0.74 ± 0.04 mg $cm^{-2}$ ($A_{geom}$). The Pt NPs account for only 0.44 ± 0.06% of the total electrode mass, which is significantly smaller than the evaluated Pt surface coverage of 15 ± 4%, resulting in a relatively large Pt mass specific surface area of 27 ± 4 $m^2$ per $g_{Pt}$. This represents ca. 40% improvement in Pt mass specific surface area and ca. 10 times lower Pt loading over other ultrathin/ultra-low loading designs that have been previously reported, such as pure Pt-OP electrodes and nanostructured thin film catalysts prepared by 3M Inc. and their collaborators (<20 $m^2$ per $g_{Pt}$).[15, 17, 19, 27]

Insight was sought into the long-term performance of the Pt coated ordered porous Au materials under electrochemical conditions, to assess the stability of the Pt NPs incorporated in the Au support, and to identify any potential routes for electrode material degradation. The Pt-coated ordered porous Au electrodes were subject to ~3.5 h of potential cycling [250 cycles between 0.05 and 1.25 V (vs. RHE) at a scan rate of 50 mV $s^{-1}$] in aqueous $H_2SO_4$ (0.5 M). Scanning electron microscopy images of the Pt-coated ordered porous Au electrodes after the 250 potential cycles (Figure S5 in Supporting Information) were consistent in appearance to those obtained before the stability test (Figure 2). Cyclic voltammetry profiles recorded between 0.05 and 1.80 V (vs. RHE) were obtained before and after this electrochemical stability test (**Figure**

**3**). First of all, the CV profiles clearly indicate that the electrode surfaces are clean and free of organic impurities after initial electrochemical cycling to remove surface contaminants (see experimental section for details), as indicated by the small double-layer capacitance ($C_{dl}$) and centering of the CV profile with respect to the baseline of current $I = 0$.[28] In the case of electrode materials containing Pt NPs, when their preparation involves organic compounds, the attainment of impurity-free CV profiles is difficult because even trace amounts of remaining organic compounds can effectively block a large portion of Pt surface sites. The CV profiles (Figure 3) exhibit features characteristic of the surface oxide formation and reduction on both Pt and Au, as well as the under-potential deposition of H ($H_{UPD}$) on Pt. Note that evaluating the potentials at which Pt surface oxidation and reduction occur is hindered by their overlap with Au oxidation and reduction, respectively, as well as relatively small $A_{ecsa,Pt}$ as compared to $A_{ecsa,Au}$ of the support. This result is expected due to the ultralow loading of the Pt NPs on the porous Au support. As a comparison, Figure S6 (Supporting Information) depicts a typical CV profile for a porous Au electrode without the Pt NPs, which is consistent with previous reports for Au electrodes.[29] This comparison does indicate that the Pt oxidation and reduction features appear to be shifted to higher and lower potentials, respectively. The features assigned to the adsorption and desorption of $H_{UPD}$ have the form of a broad wave as expected for dispersed Pt NPs. The features assigned to the $H_{UPD}$ adsorption and desorption, as well as to Pt oxide formation and reduction, are relatively small because the Pt NPs make a small contribution to the overall surface area. The results reveal that there is no significant change in CV features assigned to the adsorption and desorption of $H_{UPD}$ throughout the duration of this stability test, indicating no significant changes to the $A_{ecsa,Pt}$, and thus no substantial losses of Pt that could be assigned to the repetitive potential cycling. The stability of the Pt NPs within the Pt-coated ordered porous Au electrodes is an important characteristic of this class of materials because Pt NPs on C supports can lose up to 40% $A_{ecsa,Pt}$ under the same or similar conditions.[18, 19] Although the Au support is not ideal for all applications, the stability it provides is important to

assess the performance anticipated for this new class of ultrathin catalysts. The values for $A_{ecsa}$ of Au and Pt after the stability test were calculated to be $A_{ecsa,Au}$ = 1.2 ± 0.3 $cm^2$ and $A_{ecsa,Pt}$ = 0.24 ± 0.03 $cm^2$, respectively. It is proposed that the small increase in measured $A_{ecsa,Pt}$ (from 0.21 to 0.24 $cm^2$, thus ca. 14%) resulting from this long-term test may be due to the removal of trace levels of strongly-bonded organic contaminants. These contaminants could include residual PS or PVP originating from the template preparation process. It is proposed that these surface contaminants were not removed during the initial 20 cycles between 0.05 and 1.80 V vs. RHE intended to clean the surfaces prior to performing the stability test.[28] Due to the relatively small $H_{UPD}$ peaks, the stability of the $A_{ecsa,Pt}$ was evaluated in further detail using $CO_{chem}$ oxidative stripping voltammetry as discussed later in the manuscript.

High resolution XPS analysis before and after the stability test provides insight into changes in the chemical environment of Pt. The Pt(4f) region is most readily evaluated, with minimal interference from other components in the Pt-coated ordered porous Au electrodes, and contains two peaks corresponding to $Pt(4f)_{5/2}$ and $Pt(4f)_{7/2}$. After the 250 CV cycles, the Pt(4f) peaks are noticeably shifted to lower binding energies (**Figure 4**). Since the Au peak is not anticipated to shift, due to the large proportion of Au on the electrode surface that would be unaffected by the presence of Pt (e.g., the majority of the Au is not in contact with Pt), it is most relevant to report the shift in binding energies as the shift in the $Pt(4f)_{7/2}$ peak with respect to the $Au(4f)_{7/2}$ peak.[30] This analysis reveals a shift of 1 ± 0.1 eV to lower binding energies for the $Pt(4f)_{7/2}$ peak (relative to Au) and suggests that the Pt NPs have formed an alloy with the Au support.[31, 32] Upon forming an alloy, the Au donates further electron density to the Pt NPs leading to the observed decrease in Pt(4f) binding energy. Verification of the formation of the alloy between the Pt NPs and the Au support was sought through X-ray diffraction (XRD) analysis, but no meaningful data was obtained due to the low mass contribution of NPs within the electrode (Figure S7 in Supporting Information). To further confirm the change in composition of the Pt

NPs and their interaction with the Au support, $CO_{chem}$ oxidative stripping voltammetry experiments were performed on these materials. This electrochemical experiment is highly sensitive to changes in Pt interfacial properties, such as faceting.[33, 34] In addition, $CO_{chem}$ does not adsorb onto Au under the conditions used for the $CO_{chem}$ stripping experiments. Interference from the Au support is, therefore, minimal on the obtained voltammograms for Pt $CO_{chem}$ oxidative stripping. **Figure 5** shows the $CO_{chem}$ oxidative stripping voltammetry profiles before and after stability testing with baseline correction to remove contributions from Au and Pt oxide formation. It is well-established in literature that $CO_{chem}$ oxidation is initiated on Pt surfaces through the formation of O-containing species.[33, 34] For a polycrystalline Pt electrode, the onset potential for $CO_{chem}$ oxidative stripping is ~0.65 V and the profiles typically reveal a pre-peak and several overlapping peaks. The $CO_{chem}$ stripping voltammograms (Figure 5) show a pre-peak and two overlapping main peaks. While the intensities of the pre-peaks are comparable, the intensities of the main peaks exhibit a significant change after the stability test. This transformation may be attributed to the repetitive potential cycling of the electrode. The onset potential for $CO_{chem}$ oxidation on Pt within the as-made Pt-coated ordered porous Au electrodes is positively shifted to 0.81 V, indicating that the initiation of $CO_{chem}$ oxidation may also be inhibited. Moreover, the onset potential is even further shifted to 0.86 V after the electrochemical stability test. A change in the shape of the Pt $CO_{chem}$ oxidative stripping profile is also observed after prolonged potential cycling. A similar phenomena was observed by Friedrich *et al*., who found that the $CO_{chem}$ oxidation onset and peak maxima positively shifted as the surface coverage of small (~3-nm diameter) Pt NPs decreased on a Au support.[33] More recently, Sung *et al*. noted comparable shifts in $CO_{chem}$ oxidation on Pt and correlated these shifts to changes in the Pt(4f) XPS spectra.[32] Similarly, the positive shift observed for $CO_{chem}$ oxidative stripping voltammograms for Pt NPs in our studies could be the result of greater electron donation from the Au support. The shift in onset potential and change in $CO_{chem}$

oxidative stripping profile provide further evidence for the formation of Au-Pt alloys during the electrochemical stability test.[35]

Electrocatalytic activity of the Pt coated ordered porous Au electrodes towards ORR was evaluated by placing the electrode material on a rotating disk electrode (RDE). Linear sweep voltammograms (LSVs) of Pt-coated ordered porous Au electrodes and commercial catalyst ink electrodes were obtained in $O_2$ saturated (1.0 atm) 0.5 M $H_2SO_4$ at a rotation rate of 900 rpm (**Figure 6**; see Supporting Information for data with additional rotation rates). In this comparative analysis, both the size of the Pt NPs and the Pt mass specific surface area were kept approximately the same for the Pt-coated ordered porous Au electrodes and the commercial catalyst layers. The current generated by ORR at the Pt coated ordered porous Au electrode is primarily from the Pt NPs, because only a small current is generated due to ORR at the Au support at overpotentials ($\eta$) of >0.7 V (Figure S8 in Supporting Information). Importantly, the electrocatalytic properties of the Pt-coated ordered porous Au electrodes towards ORR remain mostly constant after the stability test (and following the observed formation of a Pt/Au alloy) (Figure S9 in Supporting Information). The onset of oxygen reduction for the Pt-coated ordered porous Au electrodes is at ~0.85 V vs. RHE, or $\eta$ = 0.4 V. This overpotential is ~0.1 V larger than that for the commercial catalyst ink electrodes; shift in onset potential of ORR for Pt/Au electrodes has been observed by others for Au-rich materials.[36-38] The binding of oxygen to the catalyst surface is known to be a key step in the electrocatalytic reduction of oxygen. Platinum is suggested to bind to adsorbed $O_2$ too strongly, as to limit the rate of removal of adsorbates and increasing $\eta$ for ORR. A correlation between the shift in the Pt oxide reduction peak and the observed ORR onset potential for Pt-coated ordered porous Au electrodes suggests that this shift in onset potential is due to electron donation from the Au support and a corresponding increase in binding strength of Pt with oxygen-containing species.[35] In the case of core-shell materials, the growth of a Pt "skin" onto

a Au core has been shown to enhance the activity of Pt towards ORR due to compressive strain effects, associated with the slight lattice mismatch between Pt and Au.[39] In addition, some previous literature on Au-Pt alloys determined that larger concentrations of Pt can exhibit greater ORR and/or MeOH oxidation reaction (MOR) electrocatalytic activity.[40] Still other literature has found that pure Pt performs better than Au-Pt alloys in acidic conditions.[38, 41] Regardless, the Pt-coated ordered porous Au electrodes were not anticipated to exhibit this enhanced behavior because they lack a core-shell morphology and the concentration of Pt is considerably less than the Au present in the OP electrode and the electrochemically formed alloy. Despite the shift in onset of ORR on the surfaces of the Pt-coated ordered porous Au electrodes, the limiting current density (per $A_{ecsa,Pt}$) achieved for Pt-coated ordered porous Au electrodes is nearly 6 times greater than that for electrodes prepared from commercial catalyst inks (Figure 6). This remarkable current density at large $\eta$ is due to the ultra-low loading of Pt at the surfaces of the Pt-coated ordered porous Au electrodes.[14] Enhanced performance at high $\eta$ for ordered porous Pt catalyst layers was also observed by Sung *et al.* and attributed to morphological advantages of the OP design.[17] This morphological advantage is not observable by RDE analyses (Figure S11 in Supporting Information), but is also anticipated for the Pt-coated ordered porous Au electrodes due to similarities in the OP morphologies of these designs. The Pt-coated ordered porous Au are, therefore, expected to have very good mass transport properties, owing to their Pt loading and open porous morphology.

Applicability of the Pt-coated ordered porous Au materials as an electrocatalyst was further assessed by monitoring their activity for the MeOH oxidation reaction (MOR). The analysis was performed by conducting CV measurements in a solution of MeOH containing electrolyte (1.0 M aqueous MeOH, 0.5 M $H_2SO_4$) and compared to the performance of a commercial catalyst ink electrode under the same conditions (**Figure 7**). The CV profiles associated with MeOH oxidation using the Pt-coated ordered porous Au electrodes and commercial catalyst

electrodes differ significantly. For example, a shift towards a lower value is observed in the onset potential from ~0.6 V to ~0.4 V and a decrease in current density (for the first forward peak) from 0.6 mA $cm^{-2}$ to 0.3 mA $cm^{-2}$ when comparing the results from the catalyst ink electrode and the Pt-coated ordered porous Au electrode, respectively. The lower current densities associated with the Pt-coated ordered porous Au electrodes for MeOH oxidation were anticipated based on previous literature,[10, 37, 42] which reports that Au-rich Au/Pt systems tend to be poor catalysts for MeOH oxidation. The second peak in the MeOH oxidation transients for the two types of electrodes has a similar onset potential. The observed decrease in the current density and shift in onset potential for the MOR could be the result of the extensive electron donation from the Au support to the Pt NPs, resulting in a change in the interactions between Pt and adsorbed oxygen-containing species.[43] A change in the interactions between adsorbed MeOH and the surfaces of the electrode is further supported by the reductive peak observed in the reverse scan from 1.25 to 0.05 V. This peak is possibly associated with formation of methyl formate species through the reductive elimination of $CO_2$ and MeOH, which has been observed for other catalysts containing an alloy of gold and platinum.[44] These results are consistent with the observed changes in potentials for $CO_{chem}$ oxidative stripping on the Pt-coated ordered porous Au electrodes in contrast to electrodes of C black supported Pt NPs. The oxidation of MeOH via reaction with adsorbed hydroxide species is, therefore, inhibited on the surfaces of Pt-coated ordered porous Au electrodes, possibly due to a larger energy barrier for removal/reaction of oxygen containing species.[45] The observed decrease in current density at the onset of MOR at the surfaces of Pt-coated ordered porous Au electrodes, combined with their enhanced Pt effective utilization for ORR electrocatalysis, suggest Pt-coated ordered porous Au electrodes could be useful as a methanol-tolerant ORR catalyst in DMFC technologies.[46]

## 3. Conclusion

Broad commercialization of low-temperature fuel cells is hindered by the under-utilization of Pt within cathodic catalyst layers. Increasing the effective utilization of Pt within these catalyst layers, through enhanced stability, increased surface area to mass ratio and good mass transport, is necessary to decrease this cost. Here we demonstrate the preparation and characterization of Pt NPs-coated ordered porous gold (Pt-coated ordered porous Au) electrodes with a large surface area to mass ratio of Pt (relative to other ultrathin Pt electrocatalyst designs) and greatly enhanced electrochemical stability over similar designs of pure Pt electrodes. A comparison of Pt-coated ordered porous Au electrodes to commercial catalyst ink electrodes prepared from C black supported Pt NPs mixed with ionomer determined that the limiting current density was greatly increased due to the low Pt loading and morphological advantages (e.g., improved mass transport) of the ordered porous electrodes, although ORR activity of Pt is decreased due to strong interactions with the Au support. The Pt-coated ordered porous Au electrodes were also shown to exhibit an increase in MeOH tolerance with a shift in the onset potential for MeOH oxidation and a low catalytic activity for MeOH oxidation. Overall, the new electrode architecture demonstrated by the Pt-coated ordered porous Au electrodes is very promising for preparing highly efficient electrocatalysts.

## 4. Experimental Section

*Preparation of OP Electrodes and Related Materials:* Platinum NPs-coated Au OP electrodes were prepared using a sacrificial polystyrene (PS) template. All solvents and chemicals purchased from either Alfa Aesar, Fisher Scientific, or Sigma-Aldrich were of high purity and were used as received. Polyvinylpyrrolidone (PVP, 55k MW, Sigma-Aldrich Co.) stabilized Pt NPs were first synthesized by literature methods with some optimizations for our research, as reported in our recent publication.[21] In brief, 6 mM $H_2PtCl_6$ prepared at least one day in advance in deionized water (5.0 mL), ethanol (40.0 mL), deionized water (5.0 mL), and

55k MW PVP (1.65 g) were combined in a round bottom flask equipped with a reflux condenser and stir bar. This solution was heated and held for 3 h at reflux under continuous stirring, forming the Pt NPs. The dimensions of the Pt NPs were assessed using ImageJ software to analyze a series of TEM images. The reported error corresponds to one standard deviation from the mean obtained from at least fifty individual NPs. The as-prepared Pt NPs were subsequently coated onto the surfaces of PS spheres (Polysciences Inc., 420-nm diameter, amine functionalized) following procedures also reported in our recent publication.[21] In brief, PS spheres were first washed by centrifugation at 15000 rpm followed by decanting of the supernatant. The isolated solids were suspended in a 1:1, v/v mixture of ethanol and water and added to the as-prepared solution of Pt NPs (with an excess of NPs). This suspension was continuously stirred for a minimum of 3 h at 55 °C. The Pt NPs-coated PS spheres were then washed 3 times through a sequential series of centrifugation, decanting of the supernatant, and dispersion of the isolated solids first into water, followed by two cycles of dispersing the isolated solids into ethanol. The density of the nanoparticle coatings were assessed via TEM image analysis of a minimum of 6 separate spheres, yielding an average and standard deviation value for the nanoparticle density over the PS sphere surfaces. The purified spheres were dried before dispersion as a suspension (~1 wt% solids) in 1-butanol (Alfa Aesar, ACS Grade). The Pt NPs-coated PS spheres were assembled at an air-water interface, as per our previous work.[19] In brief, the butanol dispersion of NPs-coated PS spheres was drop cast onto the surface of a deionized water bath held at ~55 °C until the surface was completely covered with spheres. The water bath was cooled to room temperature and three layers of the resulting close-packed assembly of Pt NPs-coated PS spheres were sequentially transferred to a polished glassy carbon disk [Pine Instrument Company, glassy carbon ChangeDisk rotating disk electrode (RDE) tip]. The use of a glassy carbon disk support allowed for control over the geometric area of the Pt-coated ordered porous Au electrodes and enabled the use of RDE for kinetic measurements. These assembled templates were dried in a vacuum desiccator overnight, rinsed with ethanol

and then dried in an oven at 70 °C for 1.0 h prior to use as a sacrificial template. Gold electrodeposition was performed with TECHNI-GOLD 25 ES solution, prepared as per manufacturer directions. Gold was deposited through the sacrificial template by pulsed electrodeposition at 38 ± 1 ºC (50 pulses, 5.0 min at 9.0 µA followed by 10 s at open circuit potential), at which point the gold deposit covered 2.5 layers of the 3-layer PS sphere assembly. The PS spheres were removed by dissolution in refluxing solvent (1:1, v/v toluene to hexanes, Sigma Aldrich, ACS Grade). Gold ordered porous electrodes were similarly prepared without the additional step of coating the PS spheres with Pt NPs prior to assembly and infiltration. This study focuses on the analysis of Pt-coated ordered porous Au electrodes that are ~2.5 pore layers thick, such that the top of the electrode consists of half-formed pores with a layer of exposed Pt NPs on the outer surfaces. This design was sought as to enable further analysis of Pt NPs by surface sensitive techniques, such as X-ray photoelectron spectroscopy.

For comparison to the Pt-coated ordered porous Au electrodes, electrodes were also prepared from an ink prepared containing commercial catalysts of C black supported Pt NPs mixed with ionomer. TEC10E50E (Tanaka Kikinzoku Kyogya Co. Ltd.) commercial catalyst ink solution containing Pt (50 wt%) and C black (50 wt%) was combined with Nafion D520 (DuPont) to create a dispersion with Pt/C black (70 wt%) and Nafion ionomer (30 wt%). This solution was ultrasonicated for ~1 h (Branson Sonic Dismembrator) to ensure complete mixing of the components. This catalyst ink solution was drop cast onto the surface of a polished glassy carbon disk electrode (3 µL volume) and dried overnight in a vacuum desiccator to evaporate all solvents. The disk and associated catalyst electrode were held at 70 °C for 1.0 h prior to use in electrocatalytic experiments to ensure that no solvent contaminants were present upon introduction to the electrochemical setup. The mass specific surface area of Pt for the catalyst ink electrode is 28 ± 3 $m^2$ per g ($A_{ecsa,Pt}$) and the Pt NPs diameter is in the range of 2 to 3 nm.

*Characterization of Electrode Structure and Composition:* Transmission electron microscopy (TEM) and scanning TEM (STEM) images of the template spheres and Pt-coated ordered porous Au electrodes were obtained using a FEI Osiris X-FEG S/TEM operating at 200 kV. The Pt NPs-coated PS sphere TEM samples were prepared by drop casting ethanol solutions of the particles onto C/Formvar 300 mesh TEM grids (Ted Pella Inc.). ImageJ software was used to analyze the percent surface area of the PS spheres covered by the Pt NPs on the prepared templates. This analysis was performed by selecting an area in which only the top surface Pt NPs were clearly visible (the thickest region with respect to the electron beam). The errors reported correspond to one standard deviation from the mean from the analysis of Pt NPs on a minimum of 10 different PS spheres. To prepare the 0.5 pore layer Pt-coated ordered porous Au electrode for TEM imaging, the electrode was fabricated onto the glassy carbon disk inserts and subsequently gently scraped from the surface with a scalpel blade. The scalpel blade, with attached pieces of the Pt-coated ordered porous Au electrode, was then dipped into a vial of water, transferring the electrode from the scalpel to the high-surface tension air-water interface. The electrode was then floated onto a 300 mesh Ni grid (Electron Microscopy Sciences). Scanning electron microscope images were acquired with a FEI Strata 235 DualBeam scanning electron microscope (SEM) operating at 10 or 15 kV before and after stability testing. Cross-section images were obtained by cutting through the Pt-coated ordered porous Au electrodes with a scalpel blade and imaging at a 45° to 60° tilt away from normal. X-ray photoelectron spectroscopy (XPS) was performed with a Kratos Analytical Axis Ultra DLD spectrometer using a monochromatic aluminum source (Al Kα, 1486.6 eV) operating at 150 W (10 mA emission current and 15 kV HT).

Inductively coupled plasma mass spectrometry analysis was conducted on a Varian 820MS (Mulgrave, Victoria, Australia) quadrupole-based ICP-MS instrument equipped with a MicroMist concentric nebulizer (Glass Expansion, Pocasset, USA) fitted into a Scott double-

pass spray chamber, which was maintained at 0 °C via a computer-controlled Peltier cooling system. The optimal plasma operating conditions and measurement parameters are provided in Table S1. Standard solutions of Au and Pt (2%, v/v) in ultrapure aqua regia (J.T. Baker, Phillipsburg, USA) were prepared from a stock multi-elemental standard solution (500 µg/L), which was made from commercially-available single element standard solutions (1000 mg/L, SCP Science, Quebec, Canada) and doubly deionized water (DDW) (Arium Pro UV/DI System, Sartorius Stedim Biotech, Goettingen, Germany). A blank and five external calibration standards (from 0.1 to 500 µg/L) were prepared in aqua regia (2% v/v). The Pt and Au from solid samples of Pt-coated ordered porous Au electrodes after material and electrochemical analysis were immersed in aqua region (1.0 mL) for 30 min, while heating to 30±1 °C. Nine mL of deionized water was then added to obtain, after thorough mixing, a 10-mL volume of sample for analysis by ICP-MS. The line of best fit obtained by linear regression analysis was then used to convert the Au and Pt count rates measured for sample solutions into Au and Pt concentrations. These concentrations were then correlated back to the original masses of Au and Pt in the Pt-coated ordered porous Au solid samples.

*Electrochemical Characterization:* Electrochemical experiments were carried out using a Princeton Applied Research model 263A potentiostat and glassware freshly cleaned by established methods.[47] A standard three-electrode setup was used, with a Pt/Pt black reversible hydrogen reference electrode (RHE), Pt gauze counter electrode and aqueous $H_2SO_4$ electrolyte (0.5 M, Fisher Scientific, ACS Reagent Grade, diluted with deionized water). The working electrodes consisted of Pt-coated ordered porous Au electrodes (ionomer-free), prepared on glassy carbon ChangeDisk RDE tips, in the Teflon shroud design prepared by Pine Instruments for the use of disk inserts with their modulated speed rotator setup. Prior to study, the electrode and Teflon shroud were subject to Soxhlet extraction in acetone for at least 3 h. High purity platinum electrode materials were supplied by Alfa Aesar (Pt ≥99.9%). The RHE electrodes

and cell used in evaluating methanol oxidation activity were prepared by Verrerie de Precision Enr. Cyclic voltammetry, oxygen reduction, and carbon monoxide oxidative stripping tests were performed using Pine Instrument's modulated speed rotator setup with associated 4-neck flask.

Carbon monoxide oxidative stripping analysis was performed before and after stability testing to detect and evaluate any changes in Pt surface structure.[34] Adsorption of $CO_{chem}$ onto the Pt surfaces was achieved by bubbling CO gas (5% CO, 95% $N_2$, 99.998% purity, Praxair) into the electrolyte (0.5 M aqueous $H_2SO_4$) while holding the electrode potential at 0.10 V (vs. RHE) for 15 min. Excess CO gas was then removed from the electrolyte by bubbling with $N_2$ gas (99.998% purity, Praxair) for 25 min. The potential was then scanned to 1.25 V (vs. RHE) at a rate of 20 mV $s^{-1}$ to oxidize adsorbed $CO_{chem}$ from the Pt surfaces, followed by 2 CV scans from 1.20 V to 0.05 V (vs. RHE) at a rate of 20 mV $s^{-1}$. The first CV scan monitored the oxidative stripping of adsorbed CO, and the second CV scan confirmed that the $CO_{chem}$ was removed from the surfaces and the electrode was free of any impurities.

Methanol oxidation experiments were performed in aqueous $H_2SO_4$ (0.5 M) containing MeOH (1.0 M, Alfa Aesar, HPLC Grade) using CV. Oxygen reduction experiments were carried out in $O_2$ saturated (1 atm) aqueous $H_2SO_4$ electrolyte (0.5 M). Electrolytes were saturated with $O_2$ by bubbling $O_2$ gas (99.98 %, Praxair) into the electrolyte for 20 min prior to experimentation and then purging the space above the electrolyte with $O_2$ gas during experimentation to maintain saturation. Oxygen reduction activity was evaluated before and after stability testing by a RDE method and cyclic voltammetry. The RDE experiments were conducted at 400, 900, 1200, 2000 and 2500 rpm, starting from 1.20 V (vs. RHE) and scanning to 0.20 V (vs. RHE) at a scan rate of 10 mV $s^{-1}$. Before each linear scan experiment, the electrode was cycled once between 0.05 and 1.80 V to remove any surface contaminants.

**Supporting Information**
Supporting Information is available from the Wiley Online Library or from the authors.

**Acknowledgements**
This work was supported in part by the Natural Sciences and Engineering Research Council (NSERC) of Canada (Grant No. 1077758) and the Canada Research Chairs Program (B.D. Gates; Grant No. 950-215846). This work made use of an ICP-MS (Queen's University) and 4D LABS (www.4dlabs.ca) shared facilities (Simon Fraser University) supported by the Canada Foundation for Innovation (CFI), British Columbia Knowledge Development Fund (BCKDF), Western Economic Diversification Canada, and Simon Fraser University. We thank Frank Orfino and Benjamin Linkewich for assisting in the preparation of the commercial catalyst layer inks.

**Conflict of Interest**
The authors declare no conflict of interest.

**References:**

[1] M. K. Debe, *Nature* **2012**, *486*, 43.
[2] J. K. Nørskov, J. Rossmeisl, A. Logadottir, L. Lindqvist, J. R. Kitchin, T. Bligaard, H. Jónsson, *The Journal of Physical Chemistry B* **2004**, *108*, 17886.
[3] T. David, in *Fuel Cell Technology Handbook*, CRC Press, 2002.
[4] a) D. Song, Q. Wang, Z. Liu, T. Navessin, M. Eikerling, S. Holdcroft, *J. Power Sources* **2004**, *126*, 104; b) Q. Wang, D. Song, T. Navessin, S. Holdcroft, Z. Liu, *Electrochim. Acta* **2004**, *50*, 725.
[5] C. Marr, X. Li, *J. Power Sources* **1999**, *77*, 17.
[6] Q. Wang, M. Eikerling, D. Song, Z.-S. Liu, *J. Electrochem. Soc.* **2007**, *154*, F95.
[7] a) S. G. Rinaldo, J. Stumper, M. Eikerling, *Journal of Physical Chemistry C* **2010**, *114*, 5773; b) F. A. de Bruijn, V. A. T. Dam, G. J. M. Janssen, *Fuel Cells* **2008**, *8*, 3; c) V. Berejnov, Z. Martin, M. West, S. Kundu, D. Bessarabov, J. Stumper, D. Susac, A. P. Hitchcock, *PCCP* **2012**, *14*, 4835.
[8] a) A. A. Topalov, I. Katsounaros, M. Auinger, S. Cherevko, J. C. Meier, S. O. Klemm, K. J. J. Mayrhofer, *Angew. Chem. Int. Ed.* **2012**, *51*, 12613; b) Y. Shao, G. Yin, Y. Gao, *J. Power Sources* **2007**, *171*, 558.
[9] S. C. Thomas, X. Ren, S. Gottesfeld, P. Zelenay, *Electrochim. Acta* **2002**, *47*, 3741.
[10] C. Lamy, C. Coutanceau, N. Alonso-Vante, in *Electrocatalysis of Direct Methanol Fuel Cells*, Wiley-VCH Verlag GmbH & Co. KGaA, 2009, 257.
[11] M. K. Debe, *ECS Trans.* **2012**, *45*, 47.
[12] D. F. van der Vliet, C. Wang, D. Tripkovic, D. Strmcnik, X. F. Zhang, M. K. Debe, R. T. Atanasoski, N. M. Markovic, V. R. Stamenkovic, *Nat Mater* **2012**, *11*, 1051.
[13] A. Rabis, P. Rodriguez, T. J. Schmidt, *ACS Catalysis* **2012**, *2*, 864.

[14] a) C. M. Zalitis, D. Kramer, A. R. Kucernak, *PCCP* **2013**, *15*, 4329; b) Y. Sun, J. Lu, L. Zhuang, *Electrochim. Acta* **2010**, *55*, 844.
[15] M. S. Wilson, S. Gottesfeld, *J. Electrochem. Soc.* **1992**, *139*, L28.
[16] U. A. Paulus, T. J. Schmidt, H. A. Gasteiger, R. J. Behm, *J. Electroanal. Chem.* **2001**, *495*, 134.
[17] O.-H. Kim, Y.-H. Cho, S. H. Kang, H.-Y. Park, M. Kim, J. W. Lim, D. Y. Chung, M. J. Lee, H. Choe, Y.-E. Sung, *Nat Commun* **2013**, *4*.
[18] J. Zhang, K. Sasaki, E. Sutter, R. R. Adzic, *Science* **2007**, *315*, 220.
[19] B. Kinkead, J. van Drunen, M. Y. Paul, K. Dowling, G. Jerkiewicz, B. Gates, *Electrocatalysis* **2013**, *4*, 179.
[20] a) J. C. Lytle, A. Stein, *ChemInform* **2010**, *41*, i; b) B. Gates, Y. Yin, Y. Xia, *Chem. Mater.* **1999**, *11*, 2827.
[21] B. K. Pilapil, M. C. P. Wang, M. T. Y. Paul, A. Nazemi, B. D. Gates, *Nanotechnology* **2014**, *26*.
[22] a) M. Behera, S. Ram, *International Nano Letters* **2013**, *3*, 1; b) R. Seoudi, A. A. Fouda, D. A. Elmenshawy, *Physica B-Condensed Matter* **2010**, *405*, 906.
[23] Y. Yin, Y. Lu, B. Gates, Y. Xia, *Chem. Mater.* **2001**, *13*, 1146.
[24] a) G. Guan, R. Zapf, G. Kolb, Y. Men, V. Hessel, H. Loewe, J. Ye, R. Zentel, *Chem. Commun.* **2007**, 260; b) J. I. L. Chen, E. Loso, N. Ebrahim, G. A. Ozin, *J. Am. Chem. Soc.* **2008**, *130*, 5420; c) C. L. Justin, S. Andreas, in *Annual Review of Nano Research*, Vol. Volume 1, World Scientific, 2006, 1; d) J. Zhang, Y. Jin, C. Li, Y. Shen, L. Han, Z. Hu, X. Di, Z. Liu, *Applied Catalysis B: Environmental* **2009**, *91*, 11.
[25] S. Tanuma, C. J. Powell, D. R. Penn, *Surf. Interface Anal.* **2011**, *43*, 689.
[26] S. Liao, B. Li, Y. Li, in *PEM Fuel Cell Electrocatalysts and Catalyst Layers*, (Ed: J. Zhang), Springer London, 2008, 487.
[27] H. A. Gasteiger, J. E. Panels, S. G. Yan, *J. Power Sources* **2004**, *127*, 162.
[28] B. E. Conway, H. Angerstein-Kozlowska, W. B. A. Sharp, E. E. Criddle, *Anal. Chem.* **1973**, *45*, 1331.
[29] a) H. Angerstein-Kozlowska, B. E. Conway, A. Hamelin, *Journal of Electroanalytical Chemistry and Interfacial Electrochemistry* **1990**, *277*, 233; b) G. Tremiliosi-Filho, L. H. Dall'Antonia, G. Jerkiewicz, *J. Electroanal. Chem.* **2005**, *578*, 1.
[30] J. Zhang, D. N. Oko, S. Garbarino, R. Imbeault, M. Chaker, A. C. Tavares, D. Guay, D. Ma, *The Journal of Physical Chemistry C* **2012**, *116*, 13413.
[31] a) X. Ge, X. Yan, R. Wang, F. Tian, Y. Ding, *The Journal of Physical Chemistry C* **2009**, *113*, 7379; b) Z. Bastl, Š. Pick, *Surf. Sci.* **2004**, *566–568, Part 2*, 832.
[32] I.-S. Park, O.-H. Kim, J. W. Kim, B. Choi, Y.-H. Cho, Y.-E. Sung, *New J. Chem.* **2015**, *39*, 6034.
[33] K. A. Friedrich, F. Henglein, U. Stimming, W. Unkauf, *Electrochim. Acta* **2000**, *45*, 3283.
[34] P. Urchaga, S. Baranton, C. Coutanceau, G. Jerkiewicz, *Langmuir* **2011**, *28*, 3658.
[35] a) N. Kristian, Y. Yu, P. Gunawan, R. Xu, W. Deng, X. Liu, X. Wang, *Electrochim. Acta* **2009**, *54*, 4916; b) B. Hammer, J. K. Nørskov, in *Advances in Catalysis*, Vol. 45 (Ed: H. K. Bruce C. Gates), Academic Press, 2000, 71.
[36] S. Guo, Y. Fang, S. Dong, E. Wang, *The Journal of Physical Chemistry C* **2007**, *111*, 17104.
[37] S. Senthil Kumar, K. L. N. Phani, *J. Power Sources* **2009**, *187*, 19.
[38] J. Luo, P. N. Njoki, Y. Lin, L. Wang, C. J. Zhong, *Electrochem. Commun.* **2006**, *8*, 581.
[39] a) M. Shao, A. Peles, K. Shoemaker, M. Gummalla, P. N. Njoki, J. Luo, C.-J. Zhong, *The Journal of Physical Chemistry Letters* **2010**, *2*, 67; b) M. Ø. Pedersen, S. Helveg, A. Ruban, I. Stensgaard, E. Lægsgaard, J. K. Nørskov, F. Besenbacher, *Surf. Sci.* **1999**, *426*, 395.

[40] a) Y. Hu, H. Zhang, P. Wu, H. Zhang, B. Zhou, C. Cai, *PCCP* **2011**, *13*, 4083; b) S.-M. Jeong, M. K. Kim, G.-P. Kim, T. Y. Kim, S.-H. Baeck, *Chem. Eng. J.* **2012**, *198–199*, 435.
[41] J. Xu, T. Zhao, Z. Liang, L. Zhu, *Chem. Mater.* **2008**, *20*, 1688.
[42] a) J. Wang, G. Yin, G. Wang, Z. Wang, Y. Gao, *Electrochem. Commun.* **2008**, *10*, 831; b) P. Hernández-Fernández, S. Rojas, P. Ocón, A. de Frutos, J. M. Figueroa, P. Terreros, M. A. Peña, J. L. G. Fierro, *J. Power Sources* **2008**, *177*, 9; c) J. Suntivich, Z. Xu, C. E. Carlton, J. Kim, B. Han, S. W. Lee, N. Bonnet, N. Marzari, L. F. Allard, H. A. Gasteiger, K. Hamad-Schifferli, Y. Shao-Horn, *J. Am. Chem. Soc.* **2013**, *135*, 7985.
[43] A. M. Hofstead-Duffy, D.-J. Chen, S.-G. Sun, Y. J. Tong, *J. Mater. Chem.* **2012**, *22*, 5205.
[44] a) *Handbook of Fuel Cells - Fundamentals, Tecnology and Applications*, Vol. 2, John Wiley and Sons, 2003; b) M. Yin, Y. Huang, L. Liang, J. Liao, C. Liu, W. Xing, *Chem. Commun.* **2011**, *47*, 8172.
[45] R. Mancharan, J. B. Goodenough, *J. Mater. Chem.* **1992**, *2*, 875.
[46] E. Antolini, T. Lopes, E. R. Gonzalez, *J. Alloys Compd.* **2008**, *461*, 253.
[47] H. Angerstein-Kozlowska, in *Comprehensive Treatise of Electrochemistry*, Vol. 9 (Ed: E. Yeager), Plenum Press, NY 1984.

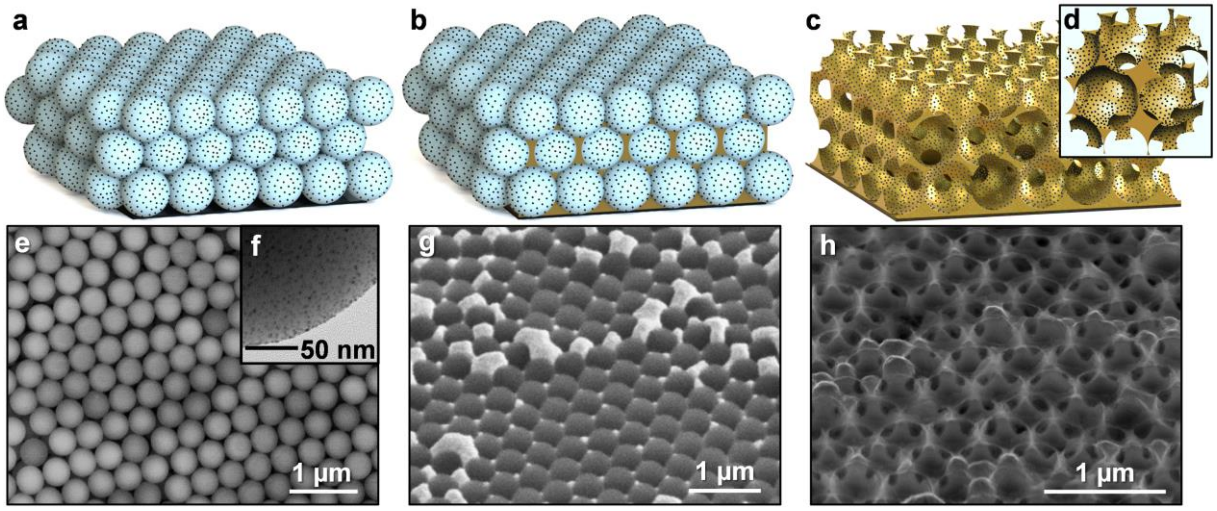


**Figure 1.** Platinum nanoparticles functionalized ordered porous gold electrodes were prepared through the use of a modular sacrificial template method. a) Polystyrene (PS) spheres coated with Pt NPs were assembled into an ordered array. b) Gold was electrodeposited through the assembly of PS spheres, filling the voids between adjacent PS spheres. c) Polystyrene spheres were dissolved in organic solvents to reveal the ordered porous structure coated with Pt NPs. d) Inset schematic shown with a higher magnification to enable a better view of the NPs that adhere to the inner surfaces of the pores within the OP electrodes. Electron microscopy images were obtained during the preparation of Pt coated ordered porous Au electrodes. e) Top view scanning electron microscopy (SEM) image of an assembly of PS spheres. f) Transmission electron microscopy (TEM) images of a section of a Pt NP coated PS sphere (dark spots on the grey hemispherical region are Pt NPs). g) SEM image of gold-filled assembly of PS spheres, viewed at 45° tilt from normal. h) SEM image of a Pt-coated ordered porous Au electrode, viewed at 60° tilt from normal.

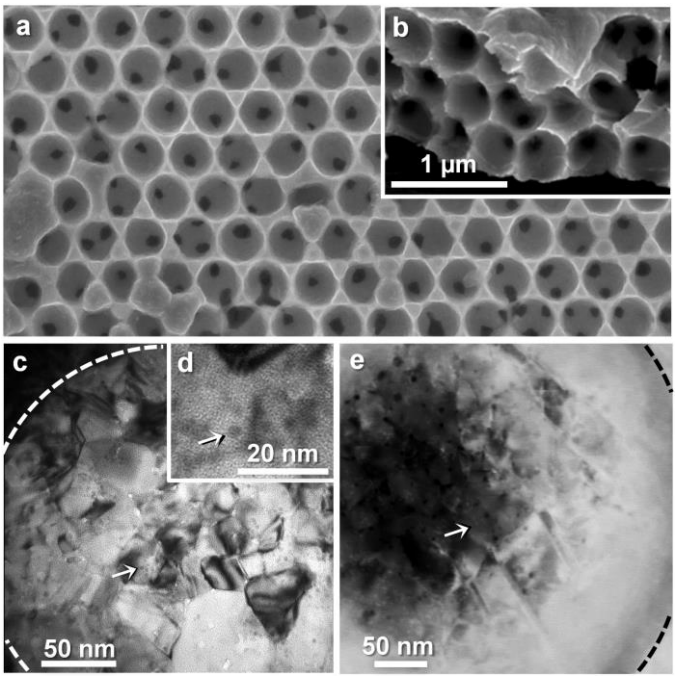


**Figure 2.** Electron microscopy images of Pt-coated ordered porous Au electrodes. Representative SEM images of Pt-coated ordered porous Au electrodes with (a) top view, and (b) cross-sectional slice at a 60° tilt from normal (1 µm scale bar applies to both SEM images). Transmission electron microscope images obtained at (c) medium and (d) high magnification, and (e) scanning TEM image as seen through the gold framework of a single pore within a Pt coated ordered porous Au electrode. Dashed lines indicate the edges of the templated pore and white arrows indicate individual Pt NPs imaged on the surfaces of the Au-OP framework.

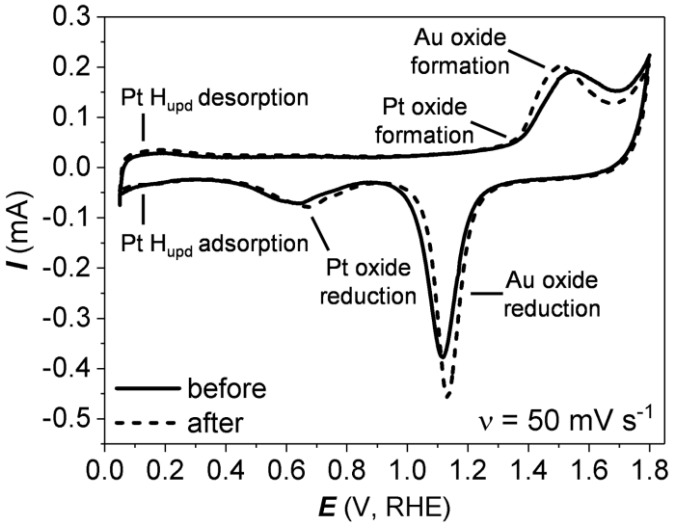


**Figure 3.** Representative cyclic voltammetry (CV) profiles of Pt-coated ordered porous Au electrodes obtained by cycling between 0.05 and 1.80 V at a scan rate of $\nu$ = 50 mV $s^{-1}$ in aqueous $H_2SO_4$ (0.5 M) before and after a stability test.

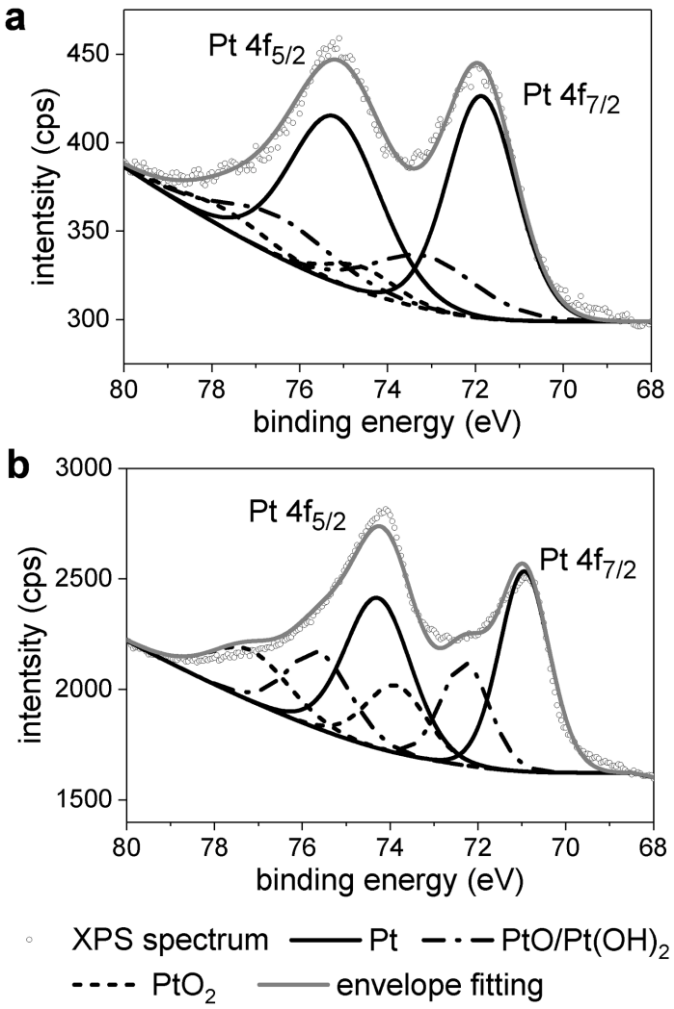


**Figure 4.** High resolution Pt(4f) X-ray photoelectron spectra with fitting analysis for Pt-coated ordered porous Au electrodes (a) before and (b) after the electrochemical stability test.

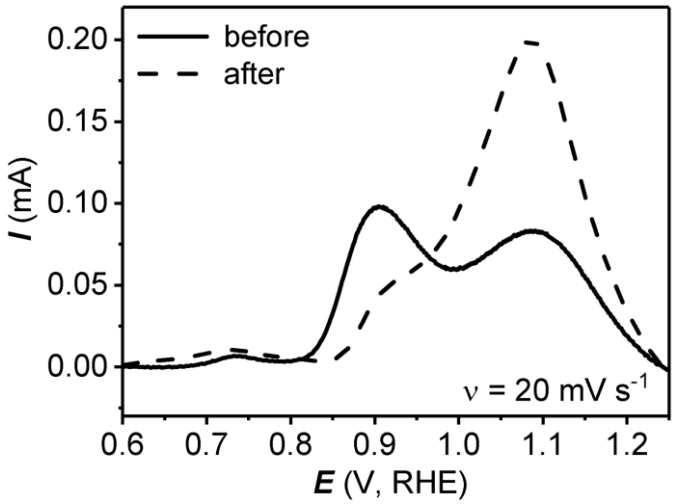


**Figure 5.** Baseline corrected Pt $CO_{chem}$ oxidative stripping voltammogram profiles of Pt-coated ordered porous Au electrodes before (solid black profile) and after (dashed profile) the electrochemical stability test. Carbon monoxide was adsorbed onto the Pt surfaces by bubbling CO gas into the electrolyte (0.5 M aqueous $H_2SO_4$), before removing excess CO gas by bubbling with $N_2$ gas. The potential was scanned to 1.20 V (vs. RHE) at a rate of 20 mV $s^{-1}$ to oxidize adsorbed $CO_{chem}$ from the Pt surfaces.

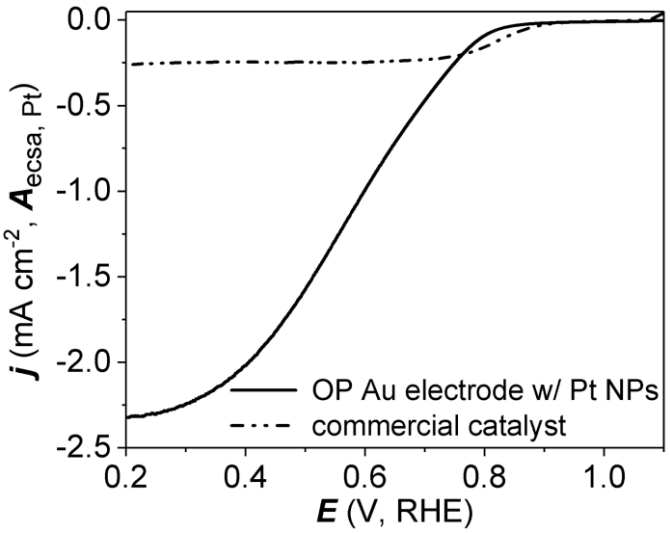


**Figure 6.** Representative rotating disk electrode (RDE) linear sweep voltammograms obtained in $O_2$ saturated electrolyte (1.0 atm, T ≈ 25 °C, 0.5 M aqueous $H_2SO_4$ at 900 rpm, ν = 10 mV $s^{-1}$) for a Pt-coated ordered porous Au electrode (solid profile) and a commercial catalyst ink electrode (dotted profile). Each sample was prepared with approximately the same Pt mass specific surface area using Pt NPs of similar diameters. Current is normalized by $A_{ecsa,Pt}$.

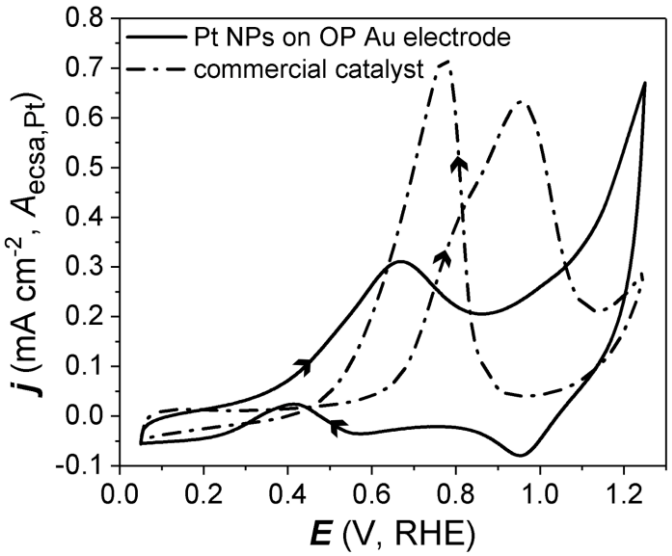


**Figure 7.** Representative CV profiles obtained in methanol (1.0 M) and $H_2SO_4$ (0.5 M) at a scan rate of 20 mV $s^{-1}$ with current normalized by $A_{ecsa,Pt}$ for a Pt-coated ordered porous Au electrode (solid profile) and a commercial catalyst ink electrode (dotted profile).

**The preparation and electrocatalytic properties of Pt nanoparticles coated on ordered porous gold electrodes are demonstrated as a route to Pt electrocatalysts with enhanced effective utilization of Pt.** These materials display good mass transport, high electrochemical stability, and a large Pt mass specific surface area in comparison to other ultrathin Pt electrocatalyst designs. The method established here for electrode preparation can be readily tuned to seek further correlations between electrocatalyst design and performance.

Keywords: platinum; electrocatalysis; inverse opal; porous electrodes; oxygen reduction reaction

Brandy K. Pilapil[1], Julia van Drunen[2], Yoseif Makonnen[2], Diane Beauchemin[2], Gregory Jerkiewicz[2], Byron D. Gates[1]*

**Ordered Porous Electrodes by Design: Towards Enhancing the Effective Utilization of Platinum in Electrocatalysis**

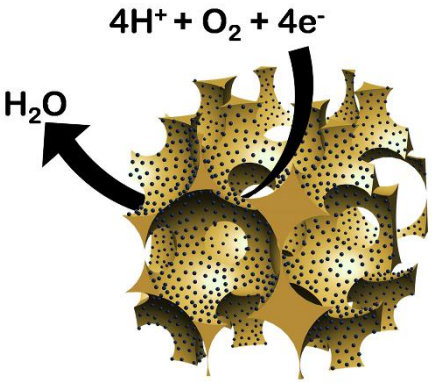

Supporting Information

# Ordered Porous Electrodes by Design: Towards Enhancing the Effective Utilization of Platinum in Electrocatalysis

*Brandy K. Pilapil, Julia van Drunen, Yoseif Makonnen, Diane Beauchemin, Gregory Jerkiewicz, Byron D. Gates**

B. K. Pilapil, B. D. Gates
Department of Chemistry and 4D LABS Simon Fraser University, 8888 University Dr. Burnaby BC, V5A 1S6, Canada

* E-mail: bgates@sfu.ca

J. van Drunen, Y. Makonnen, D. Beauchemin, G. Jerkiewicz
Department of Chemistry Queen's University, 90 Bader Lane Kingston ON, K7L 3N6, Canada

**Acknowledgements**
This work was supported in part by the Natural Sciences and Engineering Research Council (NSERC) of Canada (Grant No. 1077758) and the Canada Research Chairs Program (B.D. Gates; Grant No. 950-215846). This work made use of an ICP-MS (Queen's University) and 4D LABS (www.4dlabs.ca) shared facilities (Simon Fraser University) supported by the Canada Foundation for Innovation (CFI), British Columbia Knowledge Development Fund (BCKDF), Western Economic Diversification Canada, and Simon Fraser University. We thank Frank Orfino and Benjamin Linkewich for assisting in the preparation of the commercial catalyst layer inks.

Platinum Nanoparticle Diameter Before and After Transfer from the Sacrificial PS Template:

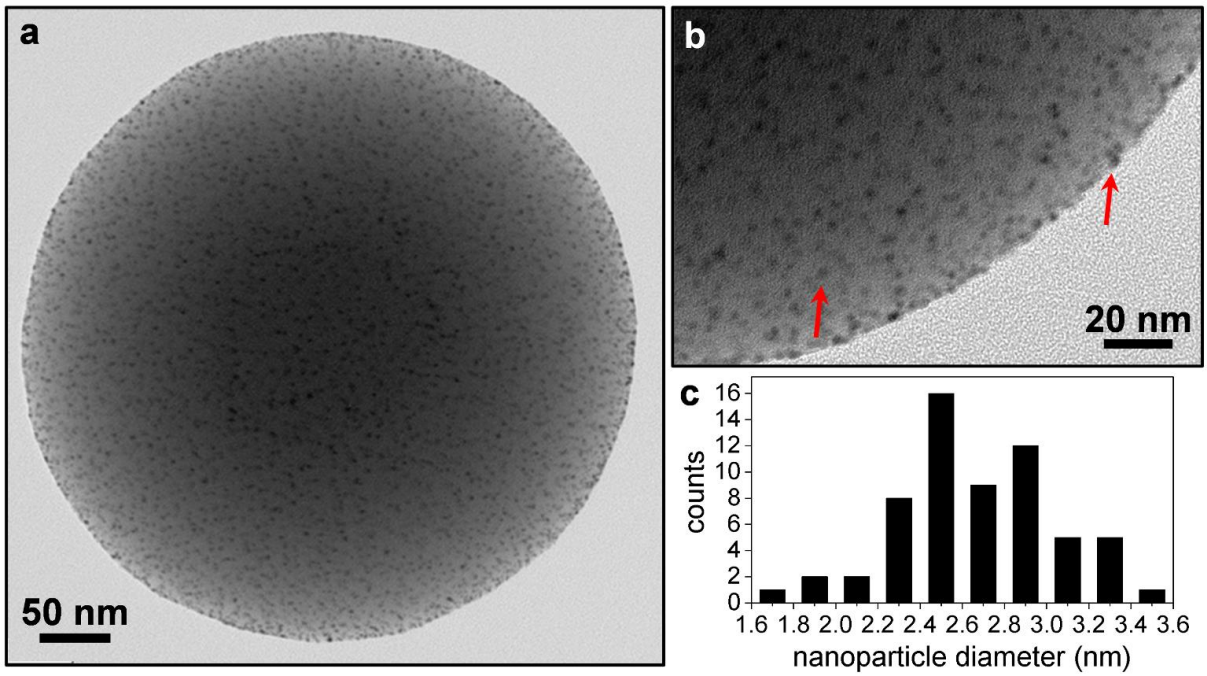


**Figure S1.** Transmission electron microscopy images of a Pt nanoparticle (NP) coated 420-nm diameter polystyrene (PS) sphere at (a) low and (b) high magnification. Red arrows point to Pt NPs on the surfaces of the PS sphere. c) Histogram depicting the distribution in measured size of the Pt NPs.

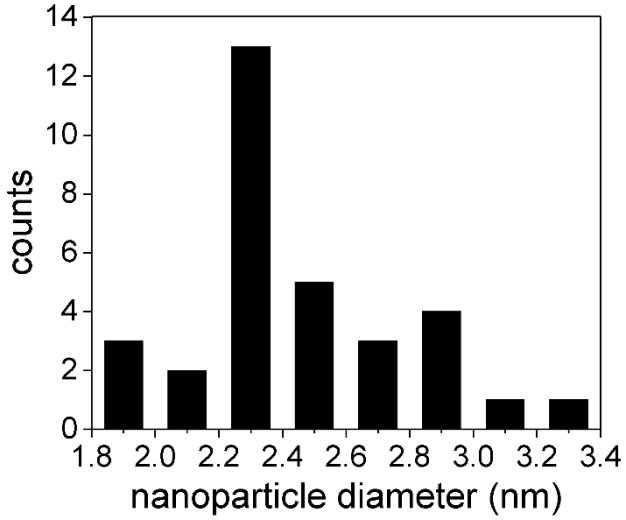


**Figure S2.** Histogram depicting the distribution in size of the Pt NPs as measured from a fragment of a Pt coated ordered porous Au electrode.

X-Ray Photoelectron Spectroscopy Survey Scan:

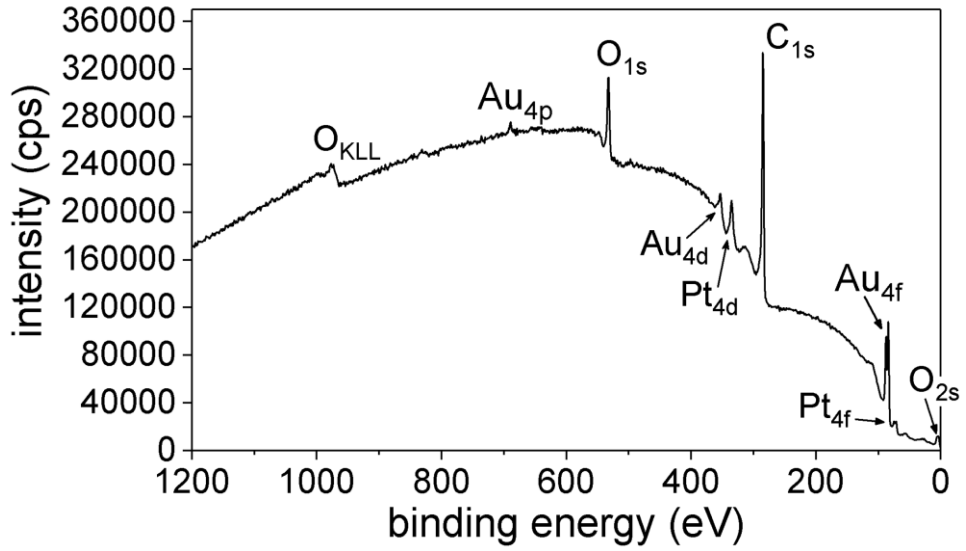


**Figure S3.** Survey X-ray photoelectron spectrum of a Pt-coated ordered porous Au electrode.

Discussion of XPS, CV and TEM Comparison for Quantitative Transfer of Platinum Nanoparticles from a Sacrificial Template:

A detailed analysis of TEM images of the Pt NP coated spherical PS templates (e.g., Figure S1) reveals that that Pt NPs cover 18 ± 4 % of the surfaces on the PS spheres. X-ray photoelectron spectroscopy survey scans of the Pt coated ordered porous Au electrodes reveal that Pt covers 15 ± 2 % of the surfaces of the Au-OP electrode. Note that the uncertainties for the XPS and CV analyses reported here were estimated based on one standard deviation from the mean from the analysis of three independently prepared Pt-coated ordered porous Au samples. The XPS value may be less accurate, due to the non-flat morphology of the electrode surfaces. Cyclic voltammetry profiles of the Pt coated ordered porous Au electrodes (Figure 3) were used to determine electrochemical surface area ($A_{ecsa}$). The $A_{ecsa}$ of Au ($A_{ecsa,Au}$) and Pt ($A_{ecsa,Pt}$) were determined to be 1.2 ± 0.3 $cm^2$ and 0.21 ± 0.03 $cm^2$, respectively. The ratio of these $A_{ecsa}$ values corresponds to a Pt surface coverage of 18 ± 3 %. The agreement in the Pt surface coverage

estimated from the XPS, CV and TEM analyses suggests that the Pt NPs were successfully and quantitatively transferred from the sacrificial spherical PS templates to the Au-OP support, while preserving the properties of the Pt NPs (e.g., particle size, surface loading, and NP-to-NP spacing). The ratio of $A_{ecsa}$ to $A_{geom}$ of the Pt-coated ordered porous Au electrodes was 6.1 ± 0.9 for Au and 1.1 ± 0.2 for Pt. This value for $A_{ecsa}$:$A_{geom}$ for Pt is quite low (~1), but can be increased through a variety of methods with minimal impact on the high mass specific surface area. Examples include increasing the thickness of the Pt coated ordered porous Au electrodes, or increasing the loading of Pt NPs on the sacrificial PS.[1,2]

High-Resolution X-Ray Photoelectron Spectroscopy — Additional Data and Analysis:

A Tougaard baseline was used for fitting analysis of Pt(4f) peaks, rather than the standard Shirley baseline, due to the overlap with the large neighboring Au(4f) peak. Fitting analysis of the Pt and Au 4f peaks was performed according to previous studies.[3,4] The percent composition of oxides remained relatively constant for both Au and Pt after electrochemical cycling (Figures 4 and S4), suggesting that the morphology (e.g., size of the Pt NPs) has not changed significantly with electrochemical cycling. The percentage of oxides on the surfaces after electrochemical cycling changes from 13 ± 3 % to 9 ± 3 % and 22 ± 3 % to 44 ± 3 % for Au and Pt, respectively. The higher coverage of oxides for Pt is anticipated due to the large relative percentage of surface area exposed to air for the Pt NPs as compared to the porous Au support; in other words, the majority of the gold is contained within the framework of these Pt coated ordered porous Au electrodes. The increase in the percent coverage of oxide for Pt NPs after the stability test may be a result of an increase in exposed surface area (due to removal of organic surface contaminants) or a result of the electrochemical treatment in aqueous $H_2SO_4$ electrolyte, which has been previously shown to form oxides detectable by XPS.[4] An increase

in the overall intensity of the XPS peaks after cycling was observed due to the removal of unavoidable surface impurities during electrochemical cycling.

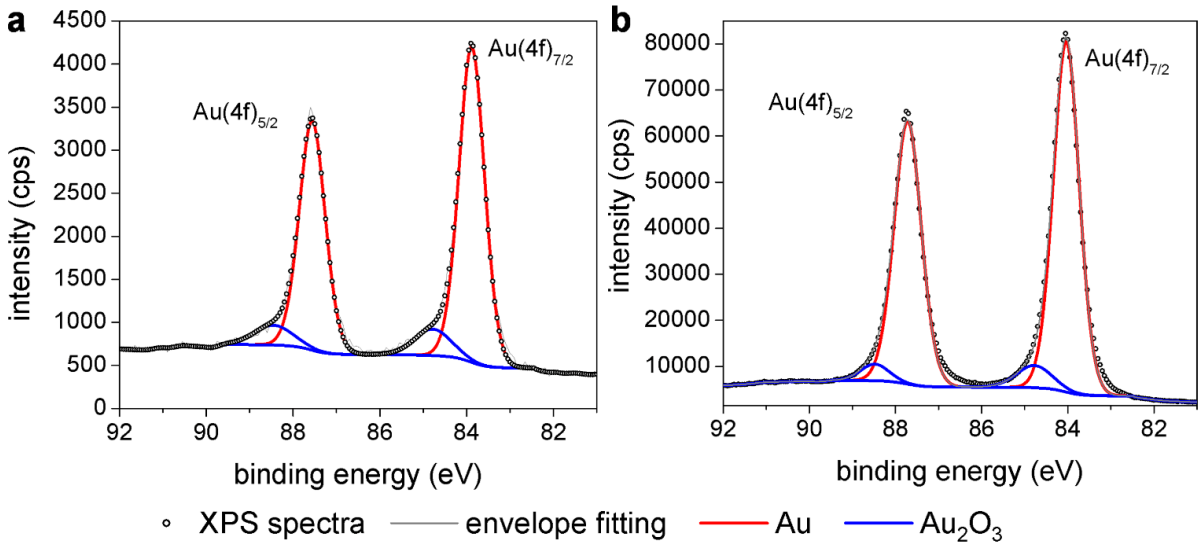


**Figure S4.** High resolution Au(4f) X-Ray photoelectron spectra of Pt-coated ordered porous Au electrodes (a) before and (b) after the electrochemical stability test with fitting analysis.

Electron Microscopy Image after the Electrochemical Stability Test:

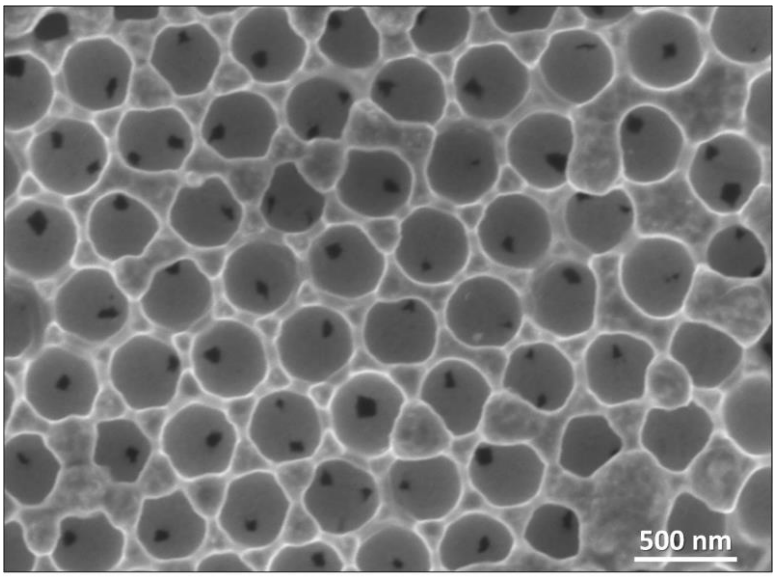


**Figure S5.** Representative SEM image of a Pt-coated ordered porous Au electrode after the electrochemical stability test.

Further Experimental Details for Electrochemical Characterization:

Unavoidable surface contaminants, which originate from the acid, ultra-high purity water, and electrode preparation methods where they are present in trace amounts, were initially removed from the electrode surface by potential cycling between 0.05 to 1.80 V (vs. RHE) at $v$ = 50 mV $s^{-1}$ for ~20 cycles, as per previous literature on the analysis of Au electrodes.[5] Prolonged potential cycling in this range resulted in dissolution of Au and Pt; Au dissolution can contribute to subsequent physical detachment of Pt NPs. Thus, cycling in this range was limited to cleaning and evaluating electrochemical surface area ($A_{ecsa}$) only.[6] $A_{ecsa}$ of Au and Pt were determined on the basis of CV analysis, as per literature methods.[7,8] The Au oxide reduction and Pt $H_{upd}$ adsorption/desorption peaks were integrated to determine the charge associated with these processes. The anodic Au oxide formation peak could not be used for this evaluation due to overlap with Pt oxide formation peak. The values for charge passed were then divided by the characteristic charge density values associated with Au oxide reduction ($q_{ox}$, 750 µC per $cm^2$) and Pt $H_{upd}$ adsorption/desorption ($q_H$, 210 µC per $cm^2$) to determine $A_{ecsa,Au}$ and $A_{ecsa,Pt}$, respectively. Note that ~2 monolayers of Au oxide is formed upon cycling to 1.80 V vs. RHE at $\nu$ = 50 mV $s^{-1}$ in aqueous $H_2SO_4$ (0.5 M), as reflected in the $q_{ox}$ value.[8] The errors reported correspond to one standard deviation from the mean following the analysis of three individual CV profiles from a representative electrode. The same trends were observed for two similarly prepared electrodes, although the exact values for $A_{ecsa}$ of Au and Pt varied slightly (approximately ± 0.3 and ± 0.1 $cm^2$, respectively).

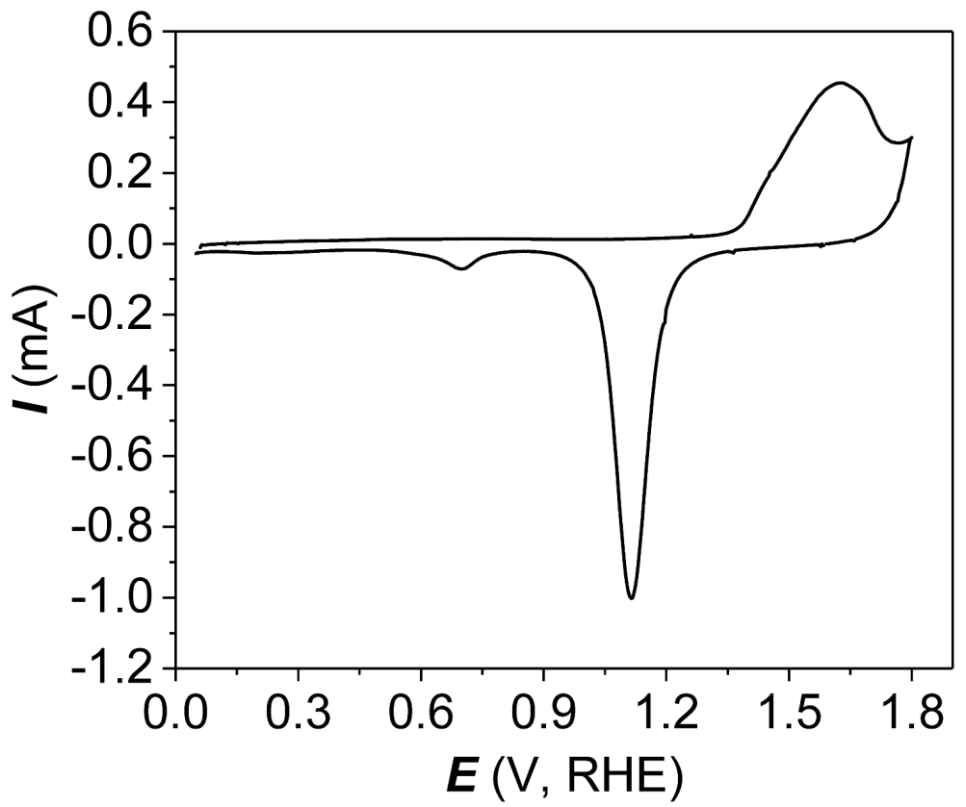


**Figure S6.** CV profile of a typical Au-OP electrode obtained in aqueous $H_2SO_4$ (0.1 M) at a scan rate of 50 mV $s^{-1}$ between 0.05 and 1.80 V vs. RHE.

X-ray Diffraction Analysis:

X-ray diffraction analysis was performed using a Rigaku Rapid-Axis Diffractometer with a Cu Kα1 radiation source (λ = 1.5406 Å). This analysis shows no evidence of platinum nanoparticles due to the low Pt concentrations within the Pt coated ordered porous electrodes.

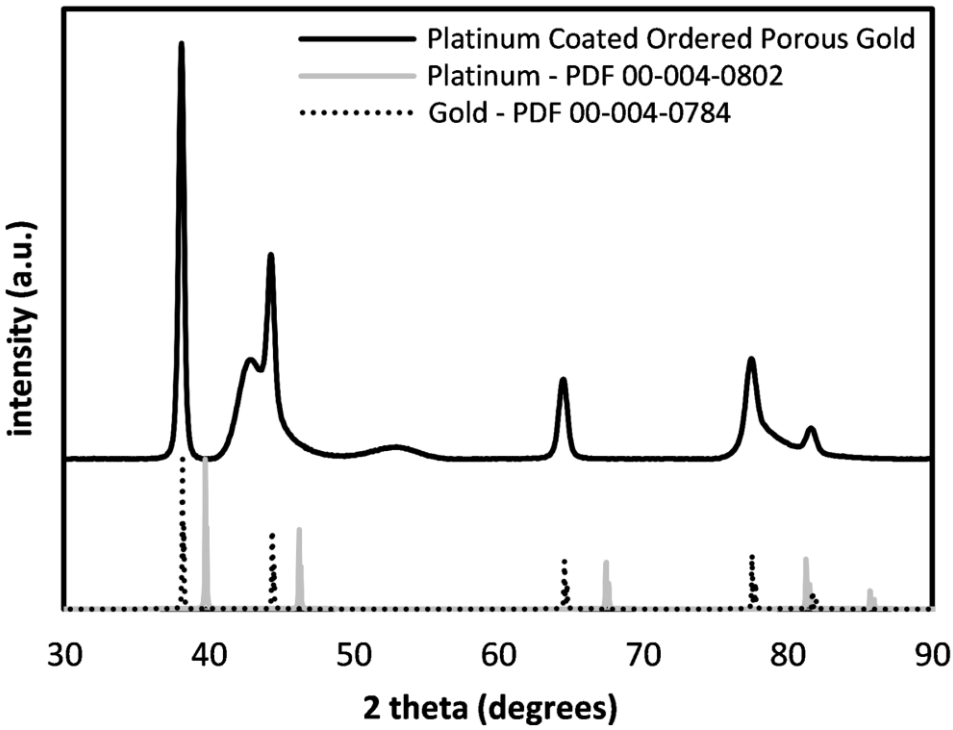


**Figure S7.** X-ray diffractogram of a Pt-coated ordered porous gold electrode and comparison to standard powder diffraction files for Au and Pt. Note that the broad peaks between 40 and 60 degrees are due to the glassy carbon support.

Carbon Monoxide Oxidative Stripping Voltammetry:

The $CO_{chem}$ oxidative stripping profile of Pt generally consists of a pre-peak, seen here between 0.6 and 0.85 V (vs. RHE), followed by a set of peaks. The presence of this pre-peak is attributed to the $CO_{chem}$ oxidative stripping proceeding according to the Eley-Rideal mechanisms.[9] The $A_{ecsa,Pt}$ was also measured from analysis of the $CO_{chem}$ oxidative stripping profile and found to be consistent with analysis of the $H_{upd}$ adsorption/desorption. Overall, results of the SEM, CV, XPS and $CO_{chem}$ oxidative stripping analyses agree, suggesting that the composition and morphology of the Pt coated ordered porous Au electrodes remains constant throughout the stability test. The constancy of $A_{ecsa,Pt}$ throughout the stability test is attributed to favorable interactions with the Au support.[10]

Oxygen Reduction Reaction Activity — Additional Data and Analysis:

Ordered porous Au (Au-OP) electrodes were prepared on gold coated silicon wafers with bare PS sphere templates, as per our previous report,[2] with a similar morphology to the Pt coated ordered porous Au electrodes. Activity of the Au-OP electrodes towards ORR was assessed after the initial removal of surface contaminants by repetitive potential cycling and obtaining CV profiles in $O_2$ saturated (1.0 atm) aqueous $H_2SO_4$ (0.5 M) at a scan rate of 20 mV $s^{-1}$ and compared to similar CV profiles for Pt coated ordered porous Au electrodes.

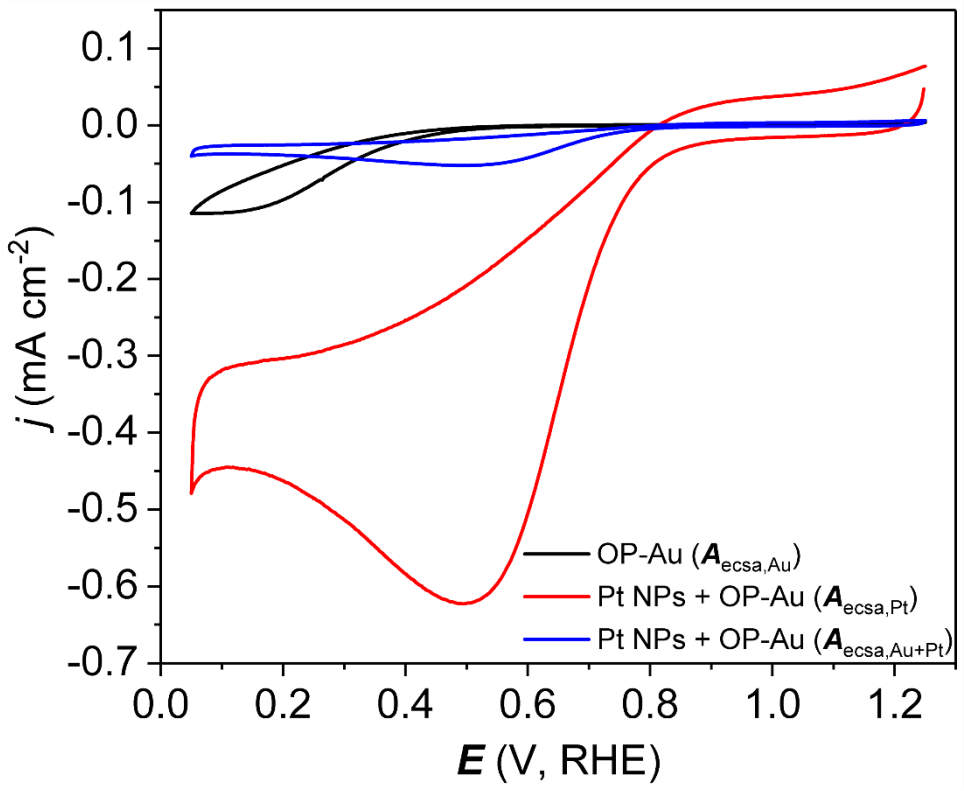


**Figure S8.** Cyclic voltammetry profiles of Au-OP and Pt-coated ordered porous Au electrodes obtained in oxygen saturated (1.0 atm) aqueous $H_2SO_4$ (0.5 M) at a scan rate of 20 mV $s^{-1}$ with current normalized by either $A_{ecsa,Au}$, $A_{ecsa,Pt}$ or the sum of $A_{ecsa,Au}$ and $A_{ecsa,Pt}$ ($A_{ecsa,Au+Pt}$).

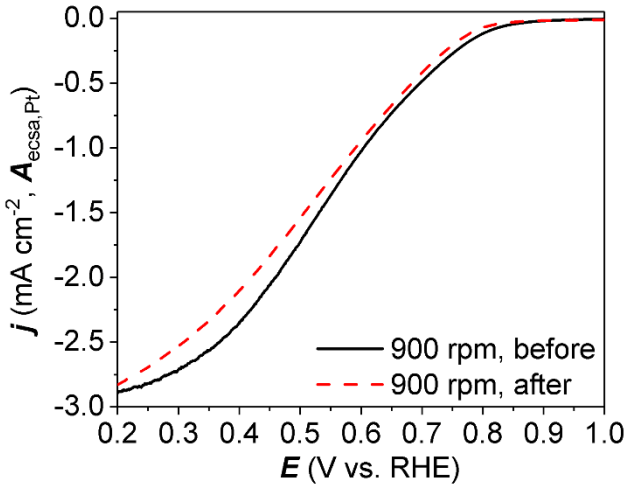


**Figure S9.** Representative RDE linear sweep voltammogram (LSV) transients for Pt-coated ordered porous Au electrodes obtained in $O_2$ saturated (1.0 atm, 0.5 M aqueous $H_2SO_4$ at 900 rpm, $\nu$ = 10 mV $s^{-1}$) before (solid transient) and after (dashed transient) the electrochemical stability test. The current is normalized by $A_{ecsa,Pt}$. Note: data presented in this figure and that in Figure 6 correspond with two separately prepared Pt-coated ordered porous Au electrodes (each of these LSVs were normalized by $A_{ecsa,Pt}$). Comparing these LSVs reveals that the profiles are relatively consistent with a small variance that may be attributed to differences in $O_2$ content, Pt-coated ordered porous Au electrode morphology and/or impurities in the electrolyte.

The kinetic parameter ($n$) quantifies the number of electrons transferred during the electrochemical reaction at our catalyst surfaces. This value can be calculated using Koutecky-Levich analysis,[11,12] and Equation (1) below:

$$\frac{1}{j} = \frac{1}{j_k} + \frac{1}{j_l} = \frac{1}{j_k} + \frac{1}{0.62nFAc_{ox}^{b}D^{2/3}\nu^{-1/6}\omega^{1/2}} \quad (1)$$

where $n$ is the kinetic parameter, $F$ is Faradays constant, $A$ is the area of the electrode ($cm^2$), $c_{ox}^{b}$ is the concentration of dissolved oxygen (~1.25 × $10^{-6}$ mol $cm^{-3}$ at 25±1 °C, 1 atm $O_2$), $D$ is the diffusion coefficient of oxygen (~1.93 × $10^{-5}$ $cm^2$ $s^{-1}$ at 25±1 °C, 1 atm $O_2$), $\nu$ is the kinematic viscosity of the solution (~0.010 $cm^2$ $s^{-1}$ for dilute aqueous solutions at 25±1 °C, 1

atm $O_2$) and ω is the rotational speed of the electrode (rad $s^{-1}$).[13] A Levich plot (plot of $1/j$ vs. $\omega^{1/2}$) enables the calculation of $n$ and $j_k$ for an electrochemical reaction of interest.[11,12] A representative linear sweep voltammogram series at different rotation rates and the corresponding Levich plot for a Pt coated ordered porous Au electrode is shown in Figure S9.

Levich plot analysis found that the kinetic parameter remained relatively constant after the stability test at 3.14 ± 0.04. A kinetic parameter of ~3 has been previously reported for a Au-rich Au/Pt electrocatalytic system[13] and indicates that ORR proceeds through a combination of direct (4 $e^-$ transfer) and indirect (2 $e^-$ transfer via a peroxide intermediate) pathways on the Pt NPs supported on OP gold.[12]

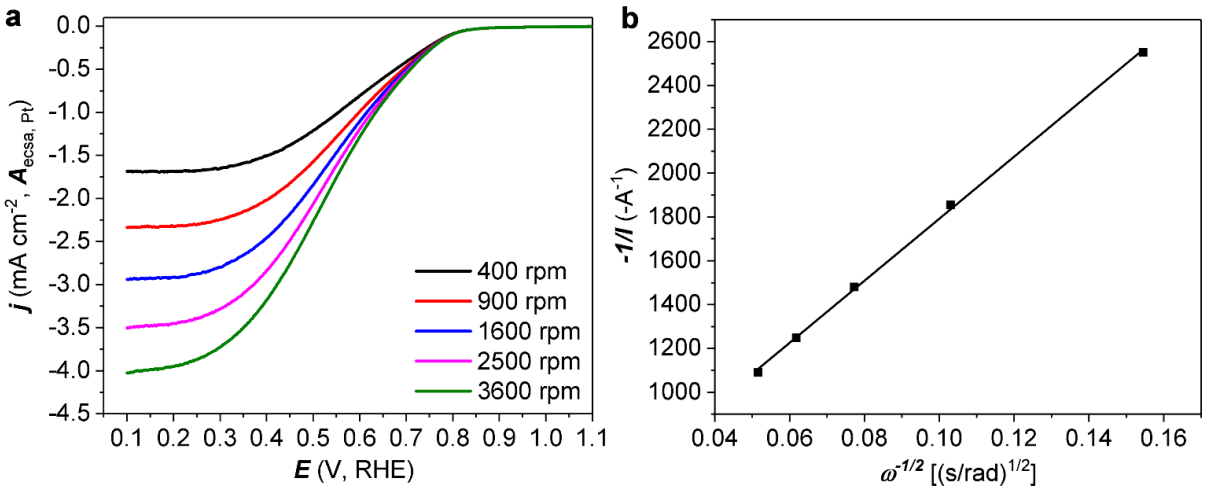


**Figure S10.** a) Linear sweep voltammograms obtained by scanning from 1.10 to 0.10 V vs. RHE in $O_2$ saturated (1.0 atm) aqueous $H_2SO_4$ (0.5 M) at $\nu = 10$ mV $s^{-1}$ at varying rotation rates using a rotating disk electrode setup. b) Levich plot derived from the linear sweep voltammograms shown in (a) for derivation of the kinetic parameter.

Platinum electrodes with varying porosity were prepared on the GC rotating disc electrodes via an analogous method to that of the Pt coated ordered porous Au electrodes for comparison. Two

electrodes of varying porosity were prepared by electrodepositing Pt to two different thicknesses, as per methods described in our previous report.[2] The first electrode is non-porous with a Pt thickness of < 100-nm, producing an array of Pt "meso-bowls". The second electrode contains Pt that is ~400-nm thick, producing an ordered porous Pt electrode (Pt-OP). Representative LSVs obtained in $O_2$ sat. (1.0 atm) aqueous $H_2SO_4$ (0.1 M) at 900 rpm are displayed in Figure S10. The "meso-bowl" type electrode exhibits a considerably larger limiting current density than the Pt-OP electrode. This result suggests that electrolyte does not penetrate into this Pt-OP electrode during RDE analysis, such that only the outer surfaces contribute to the currents measured during the LSV. As a result, the evaluated current density for the porous electrode is artificially lower, since it is normalized by the total $A_{ecsa,Pt}$ (which includes the inner pore surfaces).

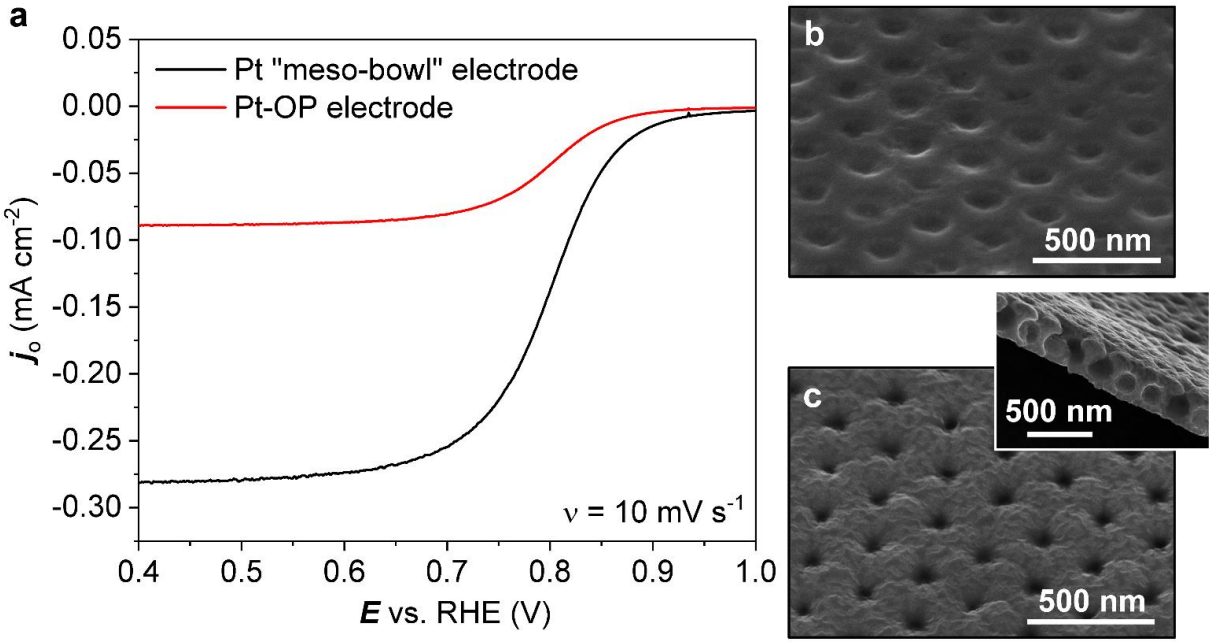


**Figure S11.** a) Representative LSVs obtained in $O_2$ sat. (1.0 atm) aqueous $H_2SO_4$ (0.1 M) at 900 rpm for an array of Pt "meso-bowls" and Pt-OP electrodes. Representative SEM images of (b) the electrodes prepared from arrays of "meso-bowls", and (c) a Pt-OP electrode (inset shows a cross-sectional view at a 60° tilt away from normal).

Mass Analysis of Pt and Au Content — Additional Experimental Details:

**Table S1.** Optimal ICP-MS operating conditions for the analysis of Pt-coated ordered porous Au samples.

| operating parameters | value |
|---|---|
| Ar plasma coolant flow rate (L/min) | 18.0 |
| Ar auxiliary flow rate (L/min) | 1.8 |
| Ar nebulizer flow rate (L/min) | 1.0 |
| Ar sheath flow rate (L/min) | 0.02 |
| R.F. power (kW) | 1.50 |
| sample uptake rate (μL/min) | 300 |
| sampling depth (mm) | 5.0 |
| 1st extraction lens (V) | -1 |
| 2nd extraction lens (V) | -167 |
| 3rd extraction lens (V) | -206 |
| corner lens (V) | -220 |
| entrance lens (V) | -2 |
| bottom mirror (V) | 32 |
| left mirror (V) | 30 |
| right mirror (V) | 24 |
| scanning mode | peak hopping |
| dwell time (μs) | 10,000 |
| analyte ions monitored | $^{197}Au^{+}$, $^{192}Pt^{+}$, $^{194}Pt^{+}$, $^{195}Pt^{+}$, $^{196}Pt^{+}$, $^{198}Pt^{+}$ |

**References:**


[1] B. K. Pilapil, M. C. P. Wang, M. T. Y. Paul, A. Nazemi, B. D. Gates, *Nanotechnology* **2014**, *26*.

[2] B. Kinkead, J. van Drunen, M. Y. Paul, K. Dowling, G. Jerkiewicz, B. D. Gates, *Electrocatalysis* **2013**, *4*, 179.

[3] a) S. D. Jackson, J. Willis, G. D. McLellan, G. Webb, M. B. T. Keegan, R. B. Moyes, S. Simpson, P. B. Wells, R. Whyman, *Journal of Catalysis* **1993**, *139*, 191; b) K. Juodkazis, J. Juodkazyt, V. Jasulaitien, A. Lukinskas, B. Šebeka, *Electrochemistry Communications* **2000**, *2*, 503; c) D. C. Lim, I. Lopez-Salido, R. Dietsche, M. Bubek, Y. D. Kim, *Surface Science* **2006**, *600*, 507.

[4] J. S. Hammond, N. Winograd, *Journal of Electroanalytical Chemistry and Interfacial Electrochemistry* **1977**, *78*, 55.

[5] M. S. El-Deab, T. Ohsaka, *Electrochemistry Communications* **2002**, *4*, 288.

[6] S. Cherevko, A. A. Topalov, A. R. Zeradjanin, I. Katsounaros, K. J. J. Mayrhofer, *RSC Advances* **2013**, *3*, 16516.

[7] a) D. Chen, Q. Tao, L. W. Liao, S. X. Liu, Y. X. Chen, S. Ye, Electrocatalysis 2011, 2, 207; b) D. A. J. Rand, R. Woods, *Journal of Electroanalytical Chemistry and Interfacial Electrochemistry* **1972**, *35*, 209.

[8] a) E. Rouya, S. Cattarin, M. L. Reed, R. G. Kelly, G. Zangari, Journal of The Electrochemical Society 2012, 159, K97; b) G. Tremiliosi-Filho, L. H. Dall'Antonia, G. Jerkiewicz, *Journal of Electroanalytical Chemistry* **2005**, *578*, 1.

[9] P. Urchaga, S. Baranton, C. Coutanceau, G. Jerkiewicz, Langmuir 2011, 28, 3658; I.-S. Park, O.-H. Kim, J. W. Kim, B. Choi, Y.-H. Cho, Y.-E. Sung, *New Journal of Chemistry* **2015**, *39*, 6034.

[10] J. Zhang, K. Sasaki, E. Sutter, R. R. Adzic, *Science* **2007**, *315*, 220.

[11] a) A. J. Bard, L. R. Faulkner, Eds., Electrochemical methods: fundamentals and applications, John Wiley and Sons, Inc., Hoboken, NJ 2000; b) Z. Qi, in PEM Fuel Cell Electrocatalysts and Catalyst Layers, (Ed: J. Zhang), Springer London, 2008, 547.

[12] a) C. Song, J. Zhang, in PEM Fuel Cell Electrocatalysts and Catalyst Layers, (Ed: J. Zhang), Springer London, 2008, 89; b) Y. Wang, P. B. Balbuena, *The Journal of Physical Chemistry B* **2005**, *109*, 14896.

[13] J. Luo, P. N. Njoki, Y. Lin, L. Wang, C. J. Zhong, *Electrochemistry Communications* **2006**, *8*, 581.